AN ADAPTIVE ALGORITHM FOR DIRECT CONVERSION RECEIVERS: ARCHITECTURE AND PERFORMANCE ANALYSIS

CAO MINGZHENG

NATIONAL UNIVERSITY OF SINGAPORE

2005

AN ADAPTIVE ALGORITHM FOR DIRECT CONVERSION RECEIVERS: ARCHITECTURE AND PERFORMANCE ANALYSIS

CAO MINGZHENG

(B. Eng)

A THESIS SUBMITTED

FOR THE DEGREE OF MASTER OF ENGINEERING

DEPARTMENT OF ELECTRICAL AND COMPUTER ENGINEERING

NATIONAL UNIVERSITY OF SINGAPORE

2005

ACKNOWLEDGEMENTS

I would like to express my utmost appreciation to both of my supervisors, Dr. Zheng Yuanjin and Prof. Hari Krishna Garg, for their invaluable guidance, continuing support and constructive suggestions throughout my research and study in the National University of Singapore and the Institute of Microelectronics. Their deep insight and wide knowledge have helped me out at the various phase of my research. It has been an enjoyable and a cultivating experience working with them.

Next, I would like to thank my great colleagues in ECE-I2R lab for all their helps and for making my study life in NUS so wonderful.

Last but not least, I would also like to thank my family members who have always been the best supports in my life.

SUMMARY

An adaptive algorithm is proposed in this thesis to remove in-phase and quadrature (I/Q) mismatch, direct current (DC) offsets, flicker noise and inter-symbol interference (ISI) simultaneously in a direct conversion receiver (DCR). I/Q mismatch is cancelled by a real valued adaptive mismatch canceller and DC offsets are removed with one complex tap. In addition, flicker noise is modeled as a complex autoregressive (AR) random process so the system to be identified transforms to an Auto Regressive with eXternal input (ARX) model. After estimating the coefficients in the model during training period, the desired signal can be estimated by using decision feedback method. To accelerate the convergence of the algorithm and to mitigate the interactions among the adaptations of the different groups of the taps of the filters, an internal iterative algorithm is introduced. Moreover, the analysis of the convergence in the mean of the taps of the proposed filters is given. Simulation results are provided to verify the superior performance of the proposed algorithm.

CONTENTS

ACKNOWLEDGEMENTS i

SUMMARY ii

LIST OF ABBREVIATIONS v

LIST OF SYMBOLS vii

LIST OF FIGURES xii

CHAPTER 1 INTRODUCTION

1.1	Outline	1
1.2	Background	1
1.3	Challenges of DCR Design	4
1.4	Previous Works on DCR Design	7
1.5	Contributions of Thesis	8
1.6	Organization of Thesis	8
1.7	Summary	9

CHAPTER 2 RECEIVED SIGNAL MODEL

2.1	Outline	11
2.2	Introduction	11
2.3	DC Offsets Model	12
2.4	Flicker Noise Model	18
2.5	I/Q Mismatch Model	20
2.6	Summary	21

CHAPTER 3 THE ADAPTIVE FILTERS AND ALGORITHM

3.1	Outline	23
3.2	Introduction	23
3.3	Architecture of the Adaptive Filters	25
3.4	Adaptive Algorithm for Distortion Mitigation	26
3.5	Internal Iterative Algorithm	32
3.6	Implementation Complexity	36
3.7	Summary	36

CHAPTER 4 CONVERGENCE ANALYSIS

4.1	Outline	38
4.2	Convergence Analysis	38
4.3	Summary	50

CHAPTER 5 SIMULATION RESULTS

5.1	Outline	51
5.2	Introduction	51
5.3	Performance of Mismatch Canceller	52
5.4	Performance of DC Offsets Canceller	53
5.5	Performance of Mismatch Canceller and DC Offsets Canceller	55
5.6	Performance of CDFE	57
5.7	Performance of the Internal Iterations	60
5.8	Comprehensive Performance of the Proposed Algorithm	61
5.9	Summary	64

CHAPTER 6 CONCLUSIONS AND FUTURE WORK

6.1	Conclusions	65
6.2	Future Work	66

REFERENCES 68

LIST OF PUBLICATIONS 70

LIST OF ABBREVIATIONS

AC:	alternate current
ADC:	analog-to-digital converter
AR:	Auto Regressive
ARX:	Auto Regressive with eXternal input
AWGN:	additive white Gaussian noise
BER:	bit error rate
BPSK:	binary phase shift keying
CDFE:	complex decision feedback equalizer
CFFE:	complex feed forward equalizer
DC:	direct current
DCR:	direct conversion receiver
DSP:	digital signal processing
FIR:	finite-impulse response
I:	in-phase
IC:	integrated circuit
IF:	intermediate frequency
I/Q :	in-phase and quadrature
ISI:	inter-symbol interference
LE:	linear equalizer

LMS:	least mean square
LNA:	low noise amplifier
LO:	local oscillator
LPF:	low pass filter
MMSE:	minimum mean-square-error
MOS:	metal oxide semiconductor
MSE:	mean-square-error
PSD:	power spectral density
Q:	quadrature
QPSK:	quadrature phase shift keying
RF:	radio frequency
SDR:	signal to constant DC offset ratio/signal to varying and constant DC offsets power ratio
SFR:	signal to flicker noise power ratio
SNR:	signal to noise power ratio
16 QAM:	16 quadrature amplitude modulation

LIST OF SYMBOLS

$\{\boldsymbol{a}_i\}$: coefficients of AR model

$\{\hat{\boldsymbol{a}}_i\}$: estimated coefficients of $\{\boldsymbol{a}_i\}$

$A(z)$: see (2-23)

$\{\boldsymbol{b}_i\}$: see (3-8)

$\{\hat{\boldsymbol{b}}_i\}$: estimated coefficients of $\{\boldsymbol{b}_i\}$

$B(z)$: $A(z)H(z)$

$\boldsymbol{c}(t)$: channel response in time domain

$C(f)$: channel response in frequency domain

$\tilde{\boldsymbol{d}}(t)$: varying DC offset

$\bar{\boldsymbol{d}}(t)$: constant DC offset

$\boldsymbol{e}(n)$: filtering error signal

$\boldsymbol{f}(t)$: flicker noise

f_c: carrier frequency

f_s: ADC sampling rate

f_0: offset frequency away from f_c

$F(z)$: $z-$transform of $\boldsymbol{f}(n)$

$g(t)$: pulse with a band-limited frequency response characteristic

$G(f)$: $g(t)$ in frequency domain

$\boldsymbol{h}(t)$: convolution of $g(t)$ and $\boldsymbol{c}(t)$

$\{\boldsymbol{h}_i\}$: coefficients of the combined channel discrete time impulse response

$H(z)$: $z-$transform of $\boldsymbol{h}(n)$

k_1: order of the CFFE taps

k_2: order of the CDFE taps

$\bar{\boldsymbol{m}}(n)$: equivalent transceiver I/Q mismatch induced signal

$\hat{m}_{1kj}(n)$: see (4-31)

$\{m_i\}$: taps of I/Q mismatch canceller

$\{m_{io}\}$: optimum values of $\{m_i\}$

$\tilde{\boldsymbol{M}}$: mismatch matrix

$\hat{\boldsymbol{M}}_1(n)$: $k_1 \times k_1$ matrix with the elements of $\hat{m}_{1kj}(n)$

n: discrete time index

$\bar{\boldsymbol{n}}(n)$: additive white Gaussian noise

$\bar{\boldsymbol{n}}'(n)$: white Gaussian noise

$N_a - 1$: order of AR model

N_h: order of channel response

$\tilde{N}$: total number of internal iterations

$\hat{P}(n)$: $\begin{pmatrix} Y'(n)\boldsymbol{t}^*(n) \\ T'(n)\boldsymbol{t}^*(n) \end{pmatrix}$

P: $E\left[\hat{P}(n)\right]$

$\hat{\boldsymbol{R}}(n)$: $\begin{bmatrix} Y'(n) \\ T'(n) \end{bmatrix}\begin{bmatrix} Y'^H(n) & T'^H(n) \end{bmatrix}$

$\boldsymbol{R}$: $E\left[\hat{\boldsymbol{R}}(n)\right]$

$\hat{\boldsymbol{R}}_{T'}(n)$: $T'(n)T'^{H}(n)$

$\hat{\boldsymbol{R}}_{XI}(n)$: $X_I(n)X_I^H(n)$

$\boldsymbol{R}_{XI}$: $E\left[\hat{\boldsymbol{R}}_{XI}(n)\right]$

$\hat{\boldsymbol{R}}_{XQ}(n)$: $X_Q(n)X_Q^H(n)$

$\boldsymbol{R}_{XQ}$: $E\left[\hat{\boldsymbol{R}}_{XQ}(n)\right]$

$\hat{\boldsymbol{R}}_{Y'}(n)$: $Y'(n)Y'^{H}(n)$

$\boldsymbol{s}(t)$: equivalent low-pass interference signal

$s_p(t)$: band-pass interference signal

$\boldsymbol{t}(m)$: discrete information-bearing sequence of symbols

$\boldsymbol{t}(n)$: training sequence

$\hat{\boldsymbol{t}}(n)$: estimated transmitted sequence

$T(z)$: $z-$transform of $\boldsymbol{t}(n)$

$T'(n)$: $\left[\boldsymbol{t}^*(n-1) \quad \boldsymbol{t}^*(n-2) \quad \ldots \quad \boldsymbol{t}^*(n-N_b+1)\right]^H$

$\boldsymbol{u}(t)$: LO signal

$\tilde{\boldsymbol{u}}(t)$: LO signal contaminated by the leakage signal

$\boldsymbol{v}(n)$: innovation of AR model

$v(t)$: equivalent low-pass transmitted signal

$V(z)$: $z-$transform of $\boldsymbol{v}(n)$

$\bar{\boldsymbol{w}}^*$: tap of DC canceller

$\left\{\hat{\boldsymbol{w}}_j^*\right\}$: taps of CFFE

$\left\{\breve{\boldsymbol{w}}_k^*\right\}$: taps of CDFE

$\bar{W}(n)$: $\left[\bar{\boldsymbol{w}}^*(n) \quad \bar{\boldsymbol{w}}^*(n-1) \quad \cdots \quad \bar{\boldsymbol{w}}^*(n-N_a+1)\right]^T$

$\widehat{W}(n)$: $\left[\widehat{\boldsymbol{w}}_0^*(n) \quad \widehat{\boldsymbol{w}}_1^*(n) \quad \cdots \quad \widehat{\boldsymbol{w}}_{N_a-1}^*(n)\right]^H$

$\breve{W}(n)$: $\left[\breve{\boldsymbol{w}}_1^*(n) \quad \breve{\boldsymbol{w}}_2^*(n) \quad \cdots \quad \breve{\boldsymbol{w}}_{N_b-1}^*(n)\right]^H$

$\boldsymbol{x}(n)$: digitalized baseband signal after the ADC to be processed by the proposed adaptive algorithm

$\tilde{\boldsymbol{x}}(t)$: equivalent low-pass received signal

$\tilde{x}_p(t)$: band-pass received signal

$\tilde{\tilde{x}}_p(t)$: received signal comtaminated by the interference signal

$\tilde{\boldsymbol{x}}'(t)$: received signal corrupted by ISI and two kinds of DC offsets

$\bar{\boldsymbol{x}}(t)$: demodulated baseband signal corrupted by ISI, two kinds of DC offsets and flicker nosie before the ADC

$\bar{\boldsymbol{x}}(n)$: samples of $\bar{\boldsymbol{x}}(t)$

$\hat{\bar{\boldsymbol{x}}}(n)$: received signal with mismatch cancelled

$\bar{\boldsymbol{x}}'(n)$: signal with mismatch and DC offsets cancelled

$X(n)$: $\left[\boldsymbol{x}^*(n) \quad \boldsymbol{x}^*(n-1) \quad \ldots \quad \boldsymbol{x}^*(n-N_a+1)\right]^H$

$X_I(n)$: real parts of $X(n)$

$X_Q(n)$: imaginary parts of $X(n)$

$\boldsymbol{y}(n)$: output of mismatch canceller

$\boldsymbol{y}'(n)$: received signal with mismatch and DC offsets cancelled

$Y'(n)$: $\left[\boldsymbol{y}'^*(n) \quad \boldsymbol{y}'^*(n-1) \quad \ldots \quad \boldsymbol{y}'^*(n-N_a+1)\right]^H$

$Y'(z)$: $z-$transform of $\boldsymbol{y}'(n)$

$\boldsymbol{z}(n)$: output signal of the proposed adaptive filter

α: amplitude gain of the I channel

β: amplitude gain of the Q channel

ϕ: phase splitter mismatch

$*$: complex conjugation

μ_b: step size for adjusting $\left\{\breve{\boldsymbol{w}}_k^*\right\}$

μ_d: step size for adjusting $\bar{\boldsymbol{w}}$

μ_f: step size for adjusting $\left\{\hat{\boldsymbol{w}}_j^*\right\}$

μ_m: step size for adjusting $\left\{m_i\right\}$

λ_{max}: maximum eigenvalue of $\boldsymbol{R}$

$\hat{\xi}(n)$: $\left|\boldsymbol{e}(n)\right|^2$

LIST OF FIGURES

Figure 1-1	Physical model of super heterodyne receiver	2
Figure 1-2	Image rejection and adjacent channel suppression	3
Figure 1-3	Physical model of DCR	4
Figure 1-4	Self-mixing of (a) LO. (b) Interferers	5
Figure 1-5	PSD of flicker noise	6
Figure 1-6	Direct conversion architecture	7
Figure 3-1	Signal flow and the proposed adaptive filter	26
Figure 5-1	BER performance of the mismatch canceller	53
Figure 5-2	BER performance of the DC offsets canceller	54
Figure 5-3	BER performance of BPSK	56
Figure 5-4	BER performance of QPSK	56
Figure 5-5	BER performance of 16 QAM	57
Figure 5-6	PSD of flicker noise and transmitted signal	59
Figure 5-7	BER performance of CDFE	59
Figure 5-8	Learning curve of the proposed algorithm without and with internal iterations	61
Figure 5-9	Comprehensive BER performance of BPSK	62
Figure 5-10	Comprehensive BER performance of QPSK	63
Figure 5-11	Comprehensive BER performance of 16QAM	63

CHAPTER 1

INTRODUCTION

1.1 Outline

In this chapter the motivations, the challenges and the previous works of the topics involved in the thesis are given, followed by the contributions and the organization of the thesis. The background is introduced in Section 1.2. Then the challenges of the direct conversion receiver (DCR) design and the previous works on DCR design are given in Section 1.3 and Section 1.4, respectively. In addition, the contributions of the thesis are given in Section 1.5. Moreover, the organization of the thesis is given in Section 1.6.

1.2 Background

Nearly all existing radio receivers are designed based on a super heterodyne architecture. They filter the received radio frequency (RF) signal and convert it to a lower intermediate frequency (IF) by mixing with an offset local oscillator (LO_1) as shown in Fig. 1-1 [1]. The IF filter is used to suppress out-of-channel interferers, performing channel selection. During the down conversion of the signal from RF to IF, an unwanted signal which is situated at an intermediate frequency above the LO_1 frequency is also translated to the IF. This undesired signal is called image signal and should be removed. The principal issue

in super heterodyne receivers is the tradeoff between the image signal rejection and the adjacent channel suppression [2].

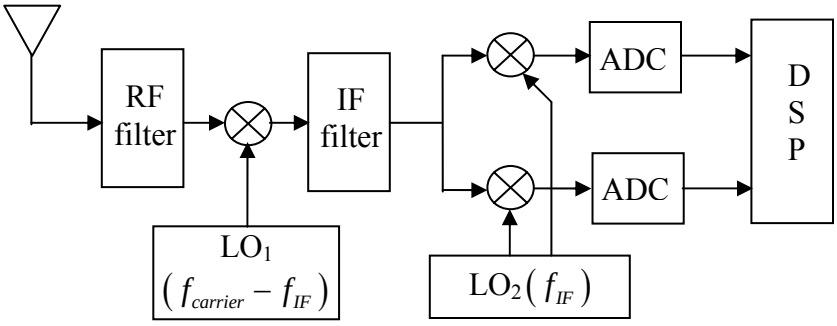

Fig. 1-1: Physical model of super heterodyne receiver.

As shown in Fig. 1-2, if the amplitude of the IF signal is high, the image is greatly attenuated but the nearby interferers remain at significant levels. On the contrary, if the amplitude of the IF signal is low, the interferers are suppressed but the image corrupts the down converted signal significantly. Consequently, both the image reject filter and the IF filter required highly selective transfer functions that are impractical in today's integrated circuit (IC) technologies. In practice, most systems utilize dual-conversion (two IF's) or a triple-conversion (three IF's) in order to achieve an acceptable compromise between the two rejections, which is at the expense of added receiver complexity and size [1] [2]. In addition, because the image reject filter is placed off-chip, a 50-Ω load is needed for the low noise amplifier (LNA) before the image reject filter. This adds another dimension to the tradeoffs among noise, linearity, gain, and power dissipation of the amplifier [2].

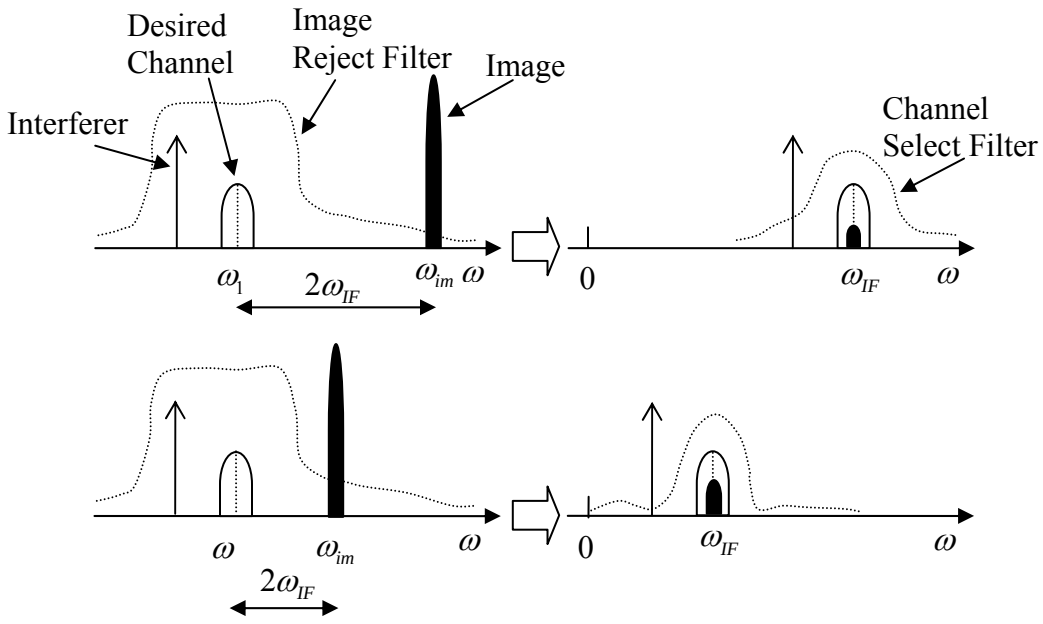

Fig. 1-2: Image rejection and adjacent channel suppression.

As shown in Fig. 1-3, If the IF signal is designed to be at frequency zero, it is called direct conversion [1] [2]. Compared to the receiver based on a super heterodyne architecture, the direct conversion receiver (DCR) has superior advantages in power dissipation, size and cost because in DCR no image reject filter is required and all IF analog components are eliminated [1] [2]. But DCR is rarely used so far due to some issues such as in-phase and quadrature (I/Q) mismatch, direct current (DC) offsets, even-order distortion and flicker noise [1] - [4]. Among these issues, DC offsets and flicker noise are generally considered more serious and challenging to the designers [2] [5]. In addition, the mismatch between the in-phase (I) and quadrature (Q) channel always exists [6]. Consequently, the methods to cancel I/Q mismatch, DC offsets and flicker noise cancellation are more frequently discussed than other issues.

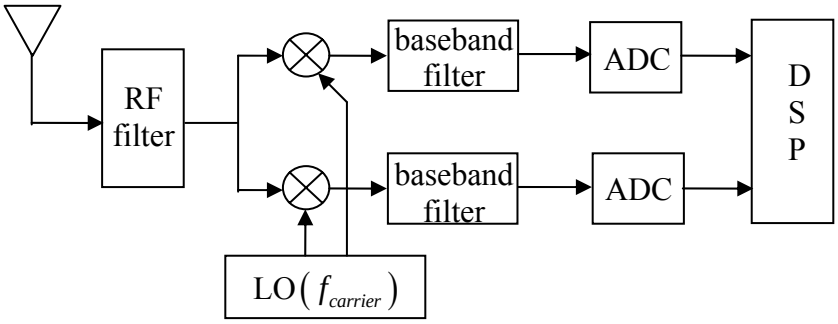

Fig. 1-3 Physical model of DCR.

1.3 Challenges of DCR Design

In a DCR, an offset voltage may appear in the signal spectrum at DC. This offset voltage value dominates the signal strength by as much as 50~100 times in amplitude and, if not removed, may substantially degrade the bit-error probability [2]. As the receiver shown in Fig. 1-4, where the low pass filter (LPF) is followed by an amplifier and an analog-to-digital converter (ADC), there are two phenomena causing DC offsets. Because the isolation between the LO port and the inputs of the mixer and the LNA is not perfect, there is a finite amount of feedthrough from the LO port to points A and B [1]. The leakage signal appearing at the inputs of the LNA and the mixer is now mixed with the LO signal, which is called self-mixing, thus producing a DC component at point C as shown in Fig. 1-4(a). Similarly, DC offset occurs if a large interferer leaks from the LNA or mixer input to the LO port and is multiplied by itself [1], as shown in Fig. 1-4(b). In addition, DC offset also can be caused by the transistor mismatch in the signal path, but DC offsets caused by this reason and the self-mixing of the interferer leakage can be

reduced to some extent by careful front-end receiver design together [7]. The comprehensive DC offsets caused by all these reasons are time-varying.

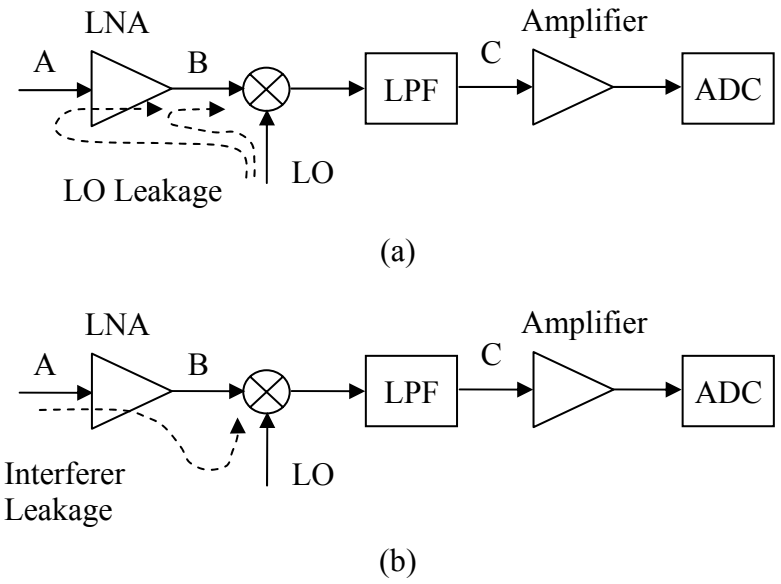

Fig. 1-4 Self-mixing of (a) LO. and (b) Interferers.

The flicker noise, also known as 1/f noise or pink noise, is an intrinsic noise phenomenon found in semiconductor devices. As the term "1/f" suggests, the noise is characterized by a power spectral density (PSD) that is inversely proportional to frequency, as shown in Fig. 1-5. In a DCR, since the downconverted spectrum is located around zero frequency, the 1/f noise of devices has a profound effect on the signal, a severe problem in metal oxide semiconductor (MOS) implementations. For example, in typical submicron MOS technologies, the total flicker noise power in a bandwidth from 10 Hz to 200 kHz can increase the noise power by 16.9 dB [1].

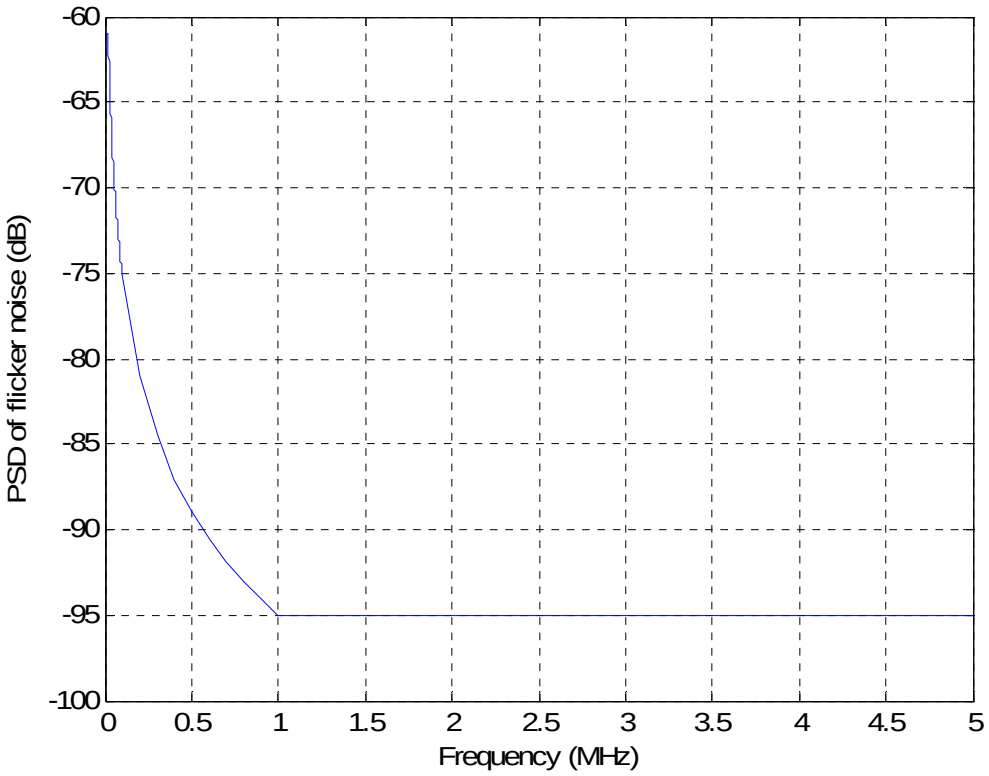

Fig. 1-5 PSD of flicker noise.

As shown in Fig. 1-6, for most phase and frequency modulation schemes, a DCR must incorporate quadrature downconversion, which requires shifting the LO output by 90^o. Due to the finite tolerances of capacitor and resistor values used to implement the analog components [6], the errors in the nominally 90^o phase shift and mismatches between the amplitudes of the I and Q signals corrupt the downconverted signal constellation [1]. The imbalance between the amplitudes of I and Q channels and the phase shift error are totally called I/Q mismatch.

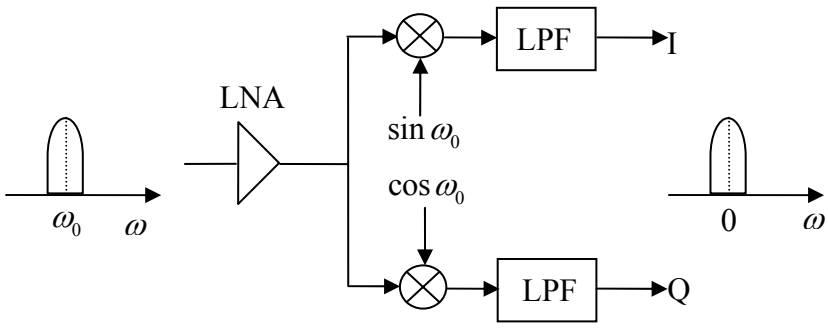

Fig. 1-6 Direct conversion architecture.

1.4 Previous Works on DCR Design

Many papers have proposed various methods to solve DC offsets and flicker noise [2] [3] [7] [8]. In [2] the DC offset is removed by employing an alternate current (AC) coupling which may distort the signals' DC components due to its high corner frequency [1] [8]; in addition, the flicker noise is regarded as equivalent in its effect to inter-symbol interference (ISI) and mitigated only by employing a finite-impulse response (FIR) minimum mean-square-error linear equalizer (MMSE-LE); moreover, it is difficult to design a suitable AC coupling because the exact 1/f roll-off frequency is unknown in practice. In [7] the varying DC component is not considered when making joint estimation of the DC offset and the radio channel. In [8] an extra averaging circuit is needed to do long-term averaging of the baseband signal to remove the DC offsets by subtracting the estimated DC value, which will increase the cost and the size of the receivers.

1.5 Contributions of the Thesis

In this thesis, a novel method to estimate the transmitted signal corrupted by ISI, I/Q mismatch, DC offsets and flicker noise is proposed. A real valued adaptive mismatch canceller is employed to cancel I/Q mismatch and the varying DC offsets are removed by one complex tap simultaneously [9] [3]. In addition, the flicker noise is modeled as a complex auto regressive (AR) random process, so the system transforms to an Auto Regressive with eXternal input (ARX) model [10]. By estimating the coefficients of the model during training period, the desired signal then can be estimated by decision feedback method. To accelerate the convergence of the algorithm, an internal iterative algorithm is introduced [9]. Moreover, the analysis of the convergence in the mean of the taps of the proposed algorithm is given. Simulation results are provided to verify the superior performance of the proposed algorithm

1.6 Organization of the Thesis

In Chapter 2, the received signal model which is the transmitted signal corrupted by channel ISI, I/Q mismatch, DC offsets and flicker noise is given. In Chapter 3, the architecture of the proposed adaptive filters is illustrated and the detailed algorithm to cancel all the previously mentioned distortions is derived. To accelerate the convergence of the algorithm, an internal iterative algorithm is introduced. In Chapter 4,

the convergence analysis in the mean of the taps is discussed. In Chapter 5, simulation results are illustrated to verify the proposed algorithm. Finally, conclusions and future work are given in Chapter 6.

1.7 Summary

Nearly all existing radio receivers are designed based on a super heterodyne architecture. The principal issue in super heterodyne receivers is the tradeoff between the image signal rejection and the adjacent channel suppression, which makes the implementation complicated. Compared to the receiver based on a super heterodyne architecture, the DCR has superior advantages in power dissipation, size and cost because in DCR no image reject filter is required and all IF analog components are eliminated. But DCR is rarely used so far due to some issues such as I/Q mismatch, DC offsets, even-order distortion and flicker noise. In DCR design, the methods to cancel I/Q mismatch, DC offsets and flicker noise cancellation are more frequently discussed than other issues. There are two phenomena causing DC offsets. One is caused by self-mixing of LO and is regarded as a constant. The other is caused by self-mixing of interferers and is time varying. The flicker noise is an intrinsic noise phenomenon found in semiconductor devices and is characterized by a PSD that is inversely proportional to frequency. The I/Q mismatch is caused by the imbalance between the amplitudes of I and Q channels and the phase shift error. In this thesis, a novel method to estimate the transmitted signal distorted by ISI, I/Q mismatch, DC offsets and flicker noise is proposed. In the following chapters,

the architecture of the proposed adaptive filters, the detailed algorithm to cancel all the previously mentioned distortions, the convergence analysis, the simulation results and the conclusions are given.

CHAPTER 2

RECEIVED SIGNAL MODEL

2.1 Outline

In this chapter the received signal model is given. In Section 2.2 the background to model the DC offsets, flicker noise and I/Q mismatch is discussed. Then the DC offsets model, flicker noise model and I/Q mismatch model are given in Section 2.3, Section 2.4 and Section 2.5, respectively.

2.2 Introduction

As mentioned in Section 1.2, in DCR design, DC offsets and flicker noise are generally considered more serious and challenging to the designers [2] [5]. In addition, the mismatch between I and Q channel always exists [6]. So this thesis focuses on I/Q mismatch, DC offsets and flicker noise cancellation.

As discussed in Section 1.3, there are two kinds of DC offsets. One is caused by self-mixing of LO and the other is caused by self-mixing of the interferences. The DC offset caused by LO changes slowly, so it is can be regarded as constant value over a packet duration. But the self-mixing caused by the signal leakage from RF input signal to

LO port generates a distortion signal whose amplitude is proportional to the RF input signal's power envelope. Consequently, these issues should be considered when modeling DC offsets.

As shown in Fig. 1-5, since flicker noise is a highly colored noise, its samples are highly correlated with one another. According to Section 1.6.3 in [11], the flicker noise can be modeled as an AR random process [12] [10].

All the received signal including the transmitted signal, DC offsets and flicker noise will be corrupted by I/Q mismatch. In this thesis a matrix similar to [4] generating I/Q mismatch is adopted.

2.3 DC Offsets Model

As mentioned in Section 1.3, there are two kinds of DC offsets. DC offset caused by self mixing of LO can be regarded as a constant value and is easily modeled. DC offset caused by self mixing of interferers is time varying and is modeled as below.

Assume that the equivalent low-pass transmitted signal has the form

$$v(t) = \sum_{m=0}^{\infty} \boldsymbol{t}(m)\, g(t - mT). \tag{2-1}$$

Here the transmission rate is $1/T$, $\{\boldsymbol{t}(m)\}$ represents the discrete information-bearing sequence of symbols and $g(t)$ is a pulse which is assumed to have a band-limited frequency response characteristic $G(f)$. In this thesis bold lower case letters represent complex variables. This signal is transmitted over a channel having a band-limited frequency response characteristic $C(f)$. Consequently the equivalent low-pass received signal can be represented as

$$\tilde{\boldsymbol{x}}(t) = \sum_{m=0}^{\infty} \boldsymbol{t}(m)\boldsymbol{h}(t - mT), \tag{2-2}$$

where

$$\boldsymbol{h}(t) = \int_{-\infty}^{+\infty} g(\tau)\boldsymbol{c}(t-\tau)d\tau\,. \tag{2-3}$$

Here $\boldsymbol{c}(t)$ is the channel response in time domain. The equivalent low-pass received signal $\tilde{\boldsymbol{x}}(t)$ can be regarded as the transmitted signal corrupted by ISI. The received signal can be written in a band-pass representation as

$$\begin{aligned}\tilde{x}_p(t) &= \mathrm{Re}\left\{\tilde{\boldsymbol{x}}(t)e^{j2\pi f_c t}\right\} \\ &= \tilde{x}_I(t)\cos(2\pi f_c t) - \tilde{x}_Q(t)\sin(2\pi f_c t)\,.\end{aligned} \tag{2-4}$$

Here $\tilde{x}_I(t)$ and $\tilde{x}_Q(t)$ denote the I and Q parts of $\tilde{\boldsymbol{x}}(t)$, respectively. f_c denotes the carrier frequency. In the thesis the subscript "I" and "Q" represent the real and imaginary parts of the variables, $\mathrm{Re}\{\bullet\}$ represents the real part of the variable.

Assume that the band-pass interference signal $s_p(t)$ is

$$\begin{aligned} s_p(t) &= \mathrm{Re}\left\{\boldsymbol{s}(t)e^{j2\pi(f_c+f_0)t}\right\} \\ &= s_I(t)\cos\left[2\pi(f_c+f_0)t\right] - s_Q(t)\sin\left[2\pi(f_c+f_0)t\right] . \end{aligned} \tag{2-5}$$

Here $\boldsymbol{s}(t)$ denotes the equivalent low-pass interference signal, $s_I(t)$ and $s_Q(t)$ denote the I and Q parts of $\boldsymbol{s}(t)$, respectively. f_0 denotes the offset frequency away from f_c.

To simplify the representation, the signals of I and Q channels of LO can be combined into a complex valued signal $\boldsymbol{u}(t)$ as

$$\begin{aligned} \boldsymbol{u}(t) &= e^{-j2\pi f_c t} \\ &= \cos(2\pi f_c t) - j\sin(2\pi f_c t). \end{aligned} \tag{2-6}$$

When incorporating the interference signal, the received signal becomes

$$\tilde{\tilde{x}}_p(t) = \tilde{x}_p(t) + s_p(t). \tag{2-7}$$

Due to the leakage of the received signal $\tilde{\tilde{x}}_p(t)$ from the RF port into the LO port as illustrated in Fig. 1-4(b), $\boldsymbol{u}(t)$ is contaminated by the leakage signal which is proportional to $\tilde{\tilde{x}}_p(t)$ by a leakage factor k ($k \ll 1$). Then the signal at the LO port becomes

$$\tilde{\boldsymbol{u}}(t) = \boldsymbol{u}(t) + k \times \left[\tilde{\tilde{x}}_p(t) - j\tilde{\tilde{x}}_p(t) \right]. \tag{2-8}$$

Here the I and Q channels of the LO signal contaminated by the leakage signal are regarded as the real and imaginary parts of a complex valued variable $\tilde{\boldsymbol{u}}(t)$, respectively. Then the signal after the mixer is

$$\begin{aligned} \tilde{\tilde{\boldsymbol{x}}}'(t) &= \tilde{\tilde{x}}_p(t) \times \tilde{\boldsymbol{u}}(t) \\ &= \left[\tilde{x}_p(t) + s_p(t) \right] \times \left\{ \boldsymbol{u}(t) + k \times \left[\tilde{\tilde{x}}_p(t) - j\tilde{\tilde{x}}_p(t) \right] \right\} \\ &= \left[\tilde{x}_p(t) + s_p(t) \right] \times \boldsymbol{u}(t) + k \times \left\{ \left[\tilde{\tilde{x}}_p(t) \right]^2 - j\left[\tilde{\tilde{x}}_p(t) \right]^2 \right\}. \end{aligned} \tag{2-9}$$

The detailed expansions of (2-9) are given as below.

$$\tilde{x}_p(t) \times \boldsymbol{u}(t) = \left[\tilde{x}_I(t) \cos(2\pi f_c t) - \tilde{x}_Q(t) \sin(2\pi f_c t) \right] \times \left[\cos(2\pi f_c t) - j \sin(2\pi f_c t) \right]$$

$$= \frac{1}{2}\left[\tilde{\boldsymbol{x}}(t) + \tilde{\boldsymbol{x}}^*(t)\cos(4\pi f_c t) - j\tilde{\boldsymbol{x}}^*(t)\sin(4\pi f_c t)\right], \tag{2-10}$$

$$s_p(t)\times \boldsymbol{u}(t) = s_I(t)\cos\left[2\pi(f_c + f_0)t\right] - s_Q(t)\sin\left[2\pi(f_c + f_0)t\right]\times e^{-j2\pi f_c t}$$

$$= \frac{1}{2}\left\{\boldsymbol{s}^*(t)\cos\left[2\pi(2f_c + f_0)t\right] - j\boldsymbol{s}^*(t)\sin\left[2\pi(2f_c + f_0)t\right]\right\}$$

$$+ \frac{1}{2}\left[\boldsymbol{s}(t)\cos(2\pi f_0 t) + j\boldsymbol{s}(t)\sin(2\pi f_0 t)\right], \tag{2-11}$$

$$\left[\tilde{\tilde{x}}_p(t)\right]^2 = \left[\tilde{x}_p(t) + s_p(t)\right]^2$$

$$= \left[\tilde{x}_p(t)\right]^2 + \left[s_p(t)\right]^2 + 2\tilde{x}_p(t)s_p(t), \tag{2-12}$$

$$\left[\tilde{x}_p(t)\right]^2 = \left[\tilde{x}_I(t)\cos(2\pi f_c t) - \tilde{x}_Q(t)\sin(2\pi f_c t)\right]^2$$

$$= \frac{1}{2}\left|\tilde{\boldsymbol{x}}(t)\right|^2 + \frac{1}{2}\left[\tilde{x}_I^2(t) - \tilde{x}_Q^2(t)\right]\cos(4\pi f_c t) - \tilde{x}_I(t)\tilde{x}_Q(t)\sin(4\pi f_c t), \tag{2-13}$$

$$\left[s_p(t)\right]^2 = \frac{1}{2}\left|\boldsymbol{s}(t)\right|^2 + \frac{1}{2}\left[s_I^2(t) - s_Q^2(t)\right]\cos\left[4\pi(f_c + f_0)t\right]$$

$$- s_I(t)s_Q(t)\sin\left[4\pi(f_c + f_0)t\right], \tag{2-14}$$

$$2\tilde{x}_p(t)s_p(t) = \left[\tilde{x}_I(t)s_I(t) - \tilde{x}_Q(t)s_Q(t)\right]\cos\left[2\pi(2f_c + f_0)t\right]$$

$$- \left[\tilde{x}_I(t)s_Q(t) + \tilde{x}_Q(t)s_I(t)\right]\sin\left[2\pi(2f_c + f_0)t\right]$$

$$+ \left[\tilde{x}_I(t)s_I(t) + \tilde{x}_Q(t)s_Q(t)\right]\cos(2\pi f_0 t)$$

$$+ \left[\tilde{x}_Q(t)s_I(t) - \tilde{x}_I(t)s_Q(t)\right]\sin(2\pi f_0 t). \tag{2-15}$$

In the thesis the superscript "*" denotes complex conjugation. The signals with high frequency in (2-9) are eliminated by LPF. Here assume f_0 is outside the LPF band. So the remaining signal after passing LPF becomes

$$\tilde{\tilde{\boldsymbol{x}}}_b'(t) = \tilde{\boldsymbol{x}}(t) + k\left\{\left[\left|\tilde{\boldsymbol{x}}(t)\right|^2 + \left|\boldsymbol{s}(t)\right|^2\right] - j\left[\left|\tilde{\boldsymbol{x}}(t)\right|^2 + \left|\boldsymbol{s}(t)\right|^2\right]\right\}. \tag{2-16}$$

It is seen in (2-16) that the mixing of $\tilde{x}_p(t)$ with the LO signal $\boldsymbol{u}(t)$ after LPF produces the ISI distorted low-pass signal $\tilde{\boldsymbol{x}}(t)$, and the mixing of $\tilde{\tilde{x}}_p(t)$ and $k\times\left[\tilde{\tilde{x}}_p(t) - j\tilde{\tilde{x}}_p(t)\right]$ after LPF produces a varying DC offset which is denoted as a complex stochastic signal $\tilde{\boldsymbol{d}}(t)$. $\tilde{\boldsymbol{d}}(t)$ can be represented as

$$\tilde{\boldsymbol{d}}(t) = k\left\{\left[\left|\tilde{\boldsymbol{x}}(t)\right|^2 + \left|\boldsymbol{s}(t)\right|^2\right] - j\left[\left|\tilde{\boldsymbol{x}}(t)\right|^2 + \left|\boldsymbol{s}(t)\right|^2\right]\right\}. \tag{2-17}$$

Similar result is given in [3]. The right hand side of (2-16) is doubled to make the factor of $\tilde{\boldsymbol{x}}(t)$ as unity.

Denote $\bar{\boldsymbol{d}}(t)$ as the DC offset caused by the self-mixing of the LO. Then the received signal in the baseband corrupted by ISI and two kinds of DC offsets can be represented as

$$\tilde{\boldsymbol{x}}'(t)=\sum_{m=0}^{\infty}\boldsymbol{t}(m)\boldsymbol{h}(t-mT)+\tilde{\boldsymbol{d}}(t)+\bar{\boldsymbol{d}}(t). \tag{2-18}$$

2.4 Flicker Noise Model

Denote $\boldsymbol{f}(t)$ as the flicker noise, then the demodulated baseband signal $\bar{\boldsymbol{x}}(t)$ before the ADC in Fig. 1-3 is the summation of ISI corrupted signal, DC offsets and flicker noise, i.e., $\bar{\boldsymbol{x}}(t)=\sum_{m=0}^{\infty}\boldsymbol{t}(m)\boldsymbol{h}(t-mT)+\tilde{\boldsymbol{d}}(t)+\bar{\boldsymbol{d}}(t)+\boldsymbol{f}(t)$. After sampling by the ADC, it can be written as

$$\bar{\boldsymbol{x}}(nT_s)=\sum_{i=0}^{N_h-1}\boldsymbol{h}_i\boldsymbol{t}\left[(n-i)T_s\right]+\tilde{\boldsymbol{d}}(nT_s)+\bar{\boldsymbol{d}}(nT_s)+\boldsymbol{f}(nT_s)\quad(\boldsymbol{h}_0=1). \tag{2-19}$$

Here n denotes the discrete time index, $f_s=1/T_s$ denotes ADC sampling rate and $t=nT_s\ (T_s=T)$; $\{\boldsymbol{h}_i\}\ (i=0,1,\cdots,N_h-1)$ are the coefficients of the combined channel discrete time impulse response; N_h is the order of channel response. (2-19) can be represented in a discrete time form as

$$\bar{\boldsymbol{x}}_n=\sum_{i=0}^{N_h-1}\boldsymbol{h}_i\boldsymbol{t}_{n-i}+\tilde{\boldsymbol{d}}_n+\bar{\boldsymbol{d}}_n+\boldsymbol{f}_n\quad(\boldsymbol{h}_0=1). \tag{2-20}$$

In the thesis, for the convenience, we will use the time index in parentheses instead of the

subscript “n” to denote the discrete sampled variables. Then (2-20) is written as

$$\bar{\boldsymbol{x}}(n)=\sum_{i=0}^{N_h-1}\boldsymbol{h}_i\boldsymbol{t}(n-i)+\tilde{\boldsymbol{d}}(n)+\bar{\boldsymbol{d}}(n)+\boldsymbol{f}(n)\quad(\boldsymbol{h}_0=1). \tag{2-21}$$

Since $\boldsymbol{f}(n)$ is a highly colored noise, it can be modeled as an AR random process as [10] [11] [12]

$$\boldsymbol{f}(n)=\sum_{i=1}^{N_a-1}(-\boldsymbol{a}_i)\,\boldsymbol{f}(n-i)+\boldsymbol{v}(n). \tag{2-22}$$

Here N_a-1 is the order, $\{\boldsymbol{a}_i\}$ $(i=1,2,\cdots,N_a-1)$ are the coefficients and $\boldsymbol{v}(n)$ is the innovation. The coefficients $\{\boldsymbol{a}_i\}$ are chosen to make the PSD of the generated $\boldsymbol{f}(n)$ close to the PSD of flicker noise. Denote $A(z)$ as

$$A(z)=1+\sum_{i=1}^{N_a-1}\boldsymbol{a}_i z^{-i}. \tag{2-23}$$

Then the $z-$transform of $\boldsymbol{f}(n)$ can be represented as

$$F(z)=\frac{V(z)}{A(z)}. \tag{2-24}$$

Here $V(z)$ is the $z-$transform of $\boldsymbol{v}(n)$ in (2-22).

2.5 I/Q Mismatch Model

Now we take the transceiver I/Q mismatch into consideration. Assume that α and β denote the amplitude gains of the I and Q channels, respectively; ϕ denotes the phase splitter mismatch and is split equally between the I and Q channels for symmetry; $\bar{\boldsymbol{m}}(n)$ denotes the equivalent transceiver I/Q mismatch induced signal; and $\bar{m}_I(n)$ and $\bar{m}_Q(n)$ denote its real and imaginary parts, respectively. Then $\bar{m}_I(n)$ and $\bar{m}_Q(n)$ can be modeled by using a matrix notation according to [4] as

$$\begin{pmatrix} \bar{m}_I(n) \\ \bar{m}_Q(n) \end{pmatrix} = \begin{pmatrix} \alpha\cos(\phi/2) & \beta\sin(\phi/2) \\ \alpha\sin(\phi/2) & \beta\cos(\phi/2) \end{pmatrix} \begin{pmatrix} \bar{x}_I(n) \\ \bar{x}_Q(n) \end{pmatrix}$$

$$= \tilde{\boldsymbol{M}} \begin{pmatrix} \bar{x}_I(n) \\ \bar{x}_Q(n) \end{pmatrix}. \qquad (2\text{-}25)$$

Here $\tilde{\boldsymbol{M}}$ represents mismatch matrix, $\bar{x}_I(n)$ and $\bar{x}_Q(n)$ represent the real and imaginary parts of $\bar{\boldsymbol{x}}(n)$, respectively.

Considering the effect of additive white Gaussian noise (AWGN) $\bar{\boldsymbol{n}}(n)$, the digitized

baseband signal after the ADC to be processed by the proposed adaptive algorithm is

$$\begin{aligned}\boldsymbol{x}(n) &= x_I(n) + jx_Q(n) \\ &= \bar{\boldsymbol{m}}(n) + \bar{\boldsymbol{n}}(n) \\ &= \left[\alpha\cos(\phi/2)\bar{x}_I(n) + \beta\sin(\phi/2)\bar{x}_Q(n)\right] \\ &\quad + j\left[\alpha\sin(\phi/2)\bar{x}_I(n) + \beta\cos(\phi/2)\bar{x}_Q(n)\right] + \bar{\boldsymbol{n}}(n).\end{aligned} \tag{2-26}$$

When $\phi = 0°$, (2-26) becomes

$$\boldsymbol{x}(n) = \alpha\bar{x}_I(n) + j\beta\bar{x}_Q(n) + \bar{\boldsymbol{n}}(n). \tag{2-27}$$

If $\alpha = \beta$, then there is no I/Q mismatch; If $\alpha \neq \beta$, it is seen that only amplitude imbalance exists.

When $\phi \neq 0°$, it is seen in (2-26) that in I channel the signal contains $\beta\sin(\phi/2)\bar{x}_Q(n)$ and in Q channel the signal contains $\alpha\sin(\phi/2)\bar{x}_I(n)$ due to the phase imbalance between I and Q channels. In this case, a mismatch canceller is needed to remove the distortion.

2.6 Summary

As mentioned in Section 1, there are two kinds of DC offsets due to the self mixing of LO and the interferers respectively. Then a constant DC offset $\bar{\boldsymbol{d}}(t)$ and a time varying DC offset $\tilde{\boldsymbol{d}}(t)$ are modeled respectively according to these two kinds of self mixings. Based on the detailed derivations, the time varying DC offset $\tilde{\boldsymbol{d}}(t)$ can be modeled as in (2-17). Because flicker noise is a highly colored noise, its samples are highly correlated with one another, consequently it can be modeled as an AR random process as (2-22). Because the I/Q mismatch can be caused by the imbalance between the amplitude gains of the I and Q channels and the phase splitter mismatch, the equivalent transceiver I/Q mismatch induced signal $\bar{\boldsymbol{m}}(n)$ can be modeled as (2-25) in which the $\bar{m}_I(n)$ and $\bar{m}_Q(n)$ are its real and imaginary parts, respectively. After considering the AWGN, the received signal model is given as in (2-26).

CHAPTER 3

THE ADAPTIVE FILTERS AND ALGORITHM

3.1 Outline

Based on the signal model in Chapter 2, the introduction of the algorithm is given in Section 3.2. The architecture of the adaptive filters proposed according to the signal model is illustrated in Section 3.3. In addition, the detailed algorithm is given in Section 3.4. To accelerate the convergence of the algorithm and to mitigate the interactions among the adaptations of the different groups of the filters' taps, an internal iterative algorithm is given in Section 3.5. Moreover, the implementation complexity of the algorithm is discussed in terms of multiplication in Section 3.6.

3.2 Introduction

According to the I/Q mismatch model in Section 2.5, when $\alpha \neq \beta$ or $\phi \neq 0°$, I/Q mismatch will occur. Based on this model, the mismatch can be mitigated by inverse modeling proposed in Section 3.6.4 in [11]. Considering that there are four elements in the matrix $\tilde{\boldsymbol{M}}$ and the assumption that the phase splitter error has been distributed equally between I and Q channels for symmetry [4], here a four real tap equalizer is

employed to model the inverse of it. Denote $\tilde{\boldsymbol{M}}^{-1}$ as the inverse of $\tilde{\boldsymbol{M}}$. According to (2-25) and (2-26), the received signal with mismatch cancelled can be represented as

$$\begin{pmatrix} \hat{\bar{x}}_I(n) \\ \hat{\bar{x}}_Q(n) \end{pmatrix} = \begin{pmatrix} \bar{x}_I(n) \\ \bar{x}_Q(n) \end{pmatrix} + \tilde{\boldsymbol{M}}^{-1} \begin{pmatrix} \bar{n}_I(n) \\ \bar{n}_Q(n) \end{pmatrix}$$

$$= \begin{pmatrix} \bar{x}_I(n) \\ \bar{x}_Q(n) \end{pmatrix} + \begin{pmatrix} \bar{n}'_I(n) \\ \bar{n}'_Q(n) \end{pmatrix}. \qquad (3\text{-}1)$$

Here $\hat{\bar{x}}_I(n)$ and $\hat{\bar{x}}_Q(n)$ denote the real and imaginary parts, respectively, of the signal $\hat{\bar{\boldsymbol{x}}}(n)$ with mismatch cancelled; $\bar{n}_I(n)$ and $\bar{n}_Q(n)$ denote the real and imaginary parts, respectively, of $\bar{\boldsymbol{n}}(n)$ in (2-26).

According to [9] [3], the varying DC offsets can be removed by one complex tap simultaneously. The signal with mismatch and DC offsets cancelled can be represented as

$$\bar{\boldsymbol{x}}'(n) = \sum_{i=0}^{N_h-1} \boldsymbol{h}_i \boldsymbol{t}(n-i) + \boldsymbol{f}(n) + \bar{\boldsymbol{n}}'(n) \quad (\boldsymbol{h}_0 = 1). \qquad (3\text{-}2)$$

Here $\bar{\boldsymbol{n}}'(n)$ is a white Gaussian noise with $\bar{n}'_I(n)$ as its real part and $\bar{n}'_Q(n)$ as its imaginary part.

We ignore $\bar{\boldsymbol{n}}'(n)$ here. Since $\boldsymbol{f}(n)$ is modeled as an AR random process, the

transmitted signal in (3-2) can be recovered by filtering $\bar{\boldsymbol{x}}'(n)$ with a complex feed forward equalizer (CFFE) and a complex decision feedback equalizer (CDFE) in sequence. The reason that $\bar{\boldsymbol{n}}'(n)$ can be ignored will be given later.

3.3 Architecture of the Adaptive Filters

Based on the system model in Chapter 2 and the discussions in Section 3.2, an integrated adaptive filter and equalizer is proposed in Fig. 3-1. It is composed of a mismatch canceller, a DC offsets canceller, a CFFE and a CDFE in sequence. The mismatch canceller is a four real tap equalizer which is to model the inverse of $\tilde{\boldsymbol{M}}$. The taps m_1 and m_4 are used to cancel the amplitude imbalance. Because phase shift error causes $x_I(n)$ to contain $\bar{x}_Q(n)$ and $x_Q(n)$ to contain $\bar{x}_I(n)$, as shown in (2-26), the tap m_2 is used to cancel the component of $\bar{x}_Q(n)$ in $x_I(n)$ and m_3 is used to cancel the component of $\bar{x}_I(n)$ in $x_Q(n)$. The output of the mismatch canceller $\boldsymbol{y}(n)$ is treated as a complex valued signal with the signal in I channel as its real part and signal in Q channel as its imaginary part. In addition, DC offsets are cancelled by a complex valued tap $\bar{\boldsymbol{w}}^*$ with 1 as the input [9] [3]. Moreover, CFFE and CDFE are employed to mitigate ISI and flicker noise.

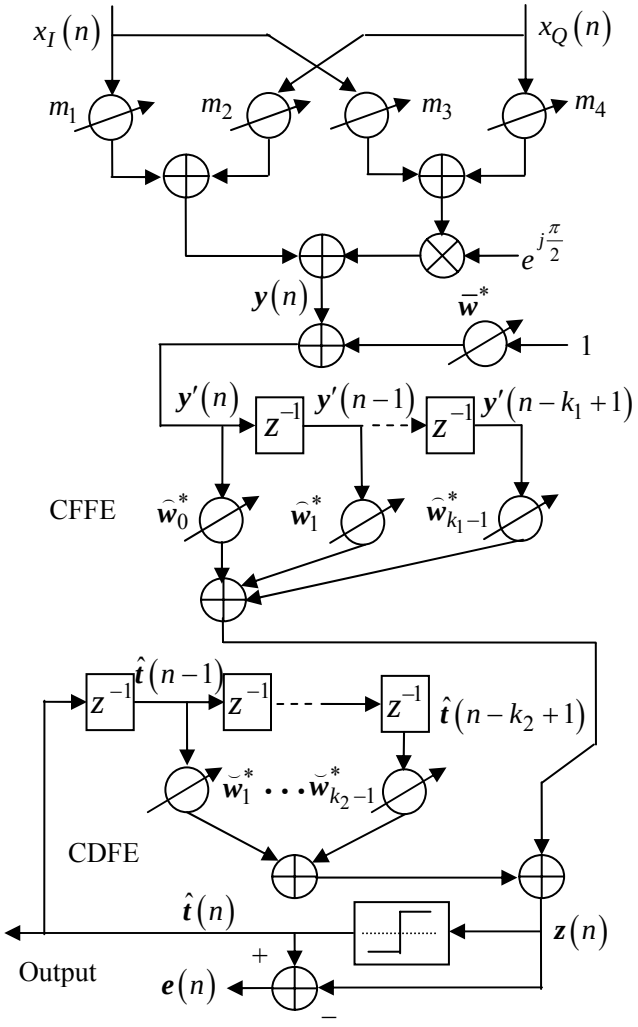

Fig. 3-1 Signal flow and the proposed adaptive filter.

3.4 Adaptive Algorithm for Distortion Mitigation

According to the model of $\boldsymbol{x}(n)$ in (2-26), the output of the mismatch canceller as shown in Fig. 3-1 is

$$\boldsymbol{y}(n) = y_I(n) + jy_Q(n), \tag{3-3}$$

$$y_I(n) = m_1(n) \times x_I(n) + m_2(n) \times x_Q(n), \tag{3-4}$$

$$y_Q(n) = m_3(n) \times x_I(n) + m_4(n) \times x_Q(n). \tag{3-5}$$

Here $\{m_i\}\ (i = 1, \cdots, 4)$ denote the taps of the mismatch canceller. Denote $\bar{\boldsymbol{w}}^*(n)$ as the tap of the DC offsets canceller, then the output $\boldsymbol{y}'(n)$ can be represented as:

$$\begin{aligned} \boldsymbol{y}'(n) &= \boldsymbol{y}(n) + \bar{\boldsymbol{w}}^*(n) \\ &= \left[y_I(n) + \bar{w}_I(n) \right] + j\left[y_Q(n) - \bar{w}_Q(n) \right]. \end{aligned} \tag{3-6}$$

Here $\bar{w}_I(n)$ and $\bar{w}_Q(n)$ denotes the real and imaginary parts of $\bar{\boldsymbol{w}}(n)$, respectively. In this thesis all the taps of the filters are given in their complex conjugation form as shown in Fig. 3-1. During the derivation of the algorithm, AWGN is dropped. When doing simulations to verify the proposed algorithm, the simulation results are still very good when AWGN exists. In addition, in practical situation the input SNR for receiver is normally high, so neglecting AWGN here is reasonable. As shown in Fig. 3-1, $\boldsymbol{y}'(n)$ can be regarded as $\boldsymbol{x}(n)$ with mismatch and DC offsets cancelled. Drop $\tilde{\boldsymbol{d}}(n)$ and $\bar{\boldsymbol{d}}(n)$, replace $\bar{\boldsymbol{x}}(n)$ with $\boldsymbol{y}'(n)$ in (2-21) and take z transform. Then according to (2-22)-(2-24), we obtain

$$A(z)Y'(z) = B(z)T(z) + V(z). \tag{3-7}$$

Here $B(z)=A(z)H(z)$, and $Y'(z)$, $T(z)$ and $H(z)$ are z transform of $\boldsymbol{y}'(n)$, $\boldsymbol{t}(n)$ and $\boldsymbol{h}(n)$, respectively. $B(z)$ can also be represented as

$$B(z)=1-\sum_{i=1}^{N_b-1}\boldsymbol{b}_i z^{-i}\ \left(N_b=N_a+N_h-1\right). \tag{3-8}$$

Since (3-7) is an ARX model, given $\boldsymbol{y}'(n)$ and $\boldsymbol{t}(n)$, the coefficients of $A(z)$ and $B(z)$ can be estimated as $\{\hat{\boldsymbol{a}}_i\}$ $(i=1,2,\cdots,N_a-1)$ and $\{\hat{\boldsymbol{b}}_i\}$ $(i=1,2,\cdots,N_b-1)$ respectively during training period. Then the desired signal can be estimated during decision period by [9] [10] [13]:

$$\hat{\boldsymbol{t}}(n)=\left(\boldsymbol{y}'(n)+\sum_{i=1}^{N_a-1}\hat{\boldsymbol{a}}_i\boldsymbol{y}'(n-i)\right)+\sum_{i=1}^{N_b-1}\hat{\boldsymbol{b}}_i\hat{\boldsymbol{t}}(n-i). \tag{3-9}$$

Here $\hat{\boldsymbol{t}}(n)$ denotes the estimated transmitted sequence $\boldsymbol{t}(n)$. As shown in Fig. 3-1, the output $\boldsymbol{z}(n)$ and the filtering error signal $\boldsymbol{e}(n)$ during training period are

$$\boldsymbol{z}(n)=\sum_{j=0}^{k_1-1}\hat{\boldsymbol{w}}_j^*(n)\,\boldsymbol{y}'(n-j)+\sum_{k=1}^{k_2-1}\breve{\boldsymbol{w}}_k^*(n)\,\boldsymbol{t}(n-k), \tag{3-10}$$

$$\boldsymbol{e}(n)=\boldsymbol{t}(n)-\boldsymbol{z}(n). \tag{3-11}$$

Here k_1 and k_2 denote the orders of the CFFE and CDFE taps, respectively, $\hat{\boldsymbol{w}}_j^*(n)$ $(j=0,1,\cdots,k_1-1)$, $\breve{\boldsymbol{w}}_k^*(n)$ $(k=,2,\cdots,k_2-1)$ and $\boldsymbol{t}(n)$ denote the CFFE tap values, CDFE tap values and the training signal, respectively. In this thesis the coefficients of $A(z)$ and $B(z)$ in (3-7) are estimated by the taps $\{\hat{\boldsymbol{w}}_j^*\}$ and $\{\breve{\boldsymbol{w}}_k^*\}$, respectively, in (3-10) by using least mean square (LMS) algorithm [10] [14]. Without loss of generality, assume $k_1 = N_a$ and $k_2 = N_b$.

Denote μ_m, μ_d, μ_f and μ_b as the step sizes for adjusting $\{m_i\}$ $(i=1,\cdots,4)$, $\bar{\boldsymbol{w}}^*$, $\{\hat{\boldsymbol{w}}_j^*\}$ $(j=0,1,\cdots,k_1-1)$ and $\{\breve{\boldsymbol{w}}_k^*\}$ $(k=,2,\cdots,k_2-1)$ respectively. According to LMS algorithm, the taps are updated as

$$m_i(n+1) = m_i(n) - \mu_m \times \nabla m_i(n) \quad (i=1,\cdots,4), \tag{3-12}$$

$$\bar{\boldsymbol{w}}^*(n+1) = \bar{\boldsymbol{w}}^*(n) - \mu_d \times \nabla \bar{\boldsymbol{w}}^*(n), \tag{3-13}$$

$$\hat{\boldsymbol{w}}_j^*(n+1) = \hat{\boldsymbol{w}}_j^*(n) - \mu_f \times \nabla \hat{\boldsymbol{w}}_j^*(n) \quad (j=0,1,\cdots,k_1-1), \tag{3-14}$$

$$\breve{\boldsymbol{w}}_k^*(n+1) = \breve{\boldsymbol{w}}_k^*(n) - \mu_b \times \nabla \breve{\boldsymbol{w}}_k^*(n) \quad (k=1,2,\cdots,k_2-1). \tag{3-15}$$

$\{\nabla m_i\}$, $\nabla \bar{\boldsymbol{w}}^*$, $\{\nabla \hat{\boldsymbol{w}}_j^*\}$ and $\{\nabla \breve{\boldsymbol{w}}_k^*\}$ can be derived by taking partial derivatives of $|\boldsymbol{e}(n)|^2$ with respect to $\{m_i\}$, $\bar{\boldsymbol{w}}^*$, $\{\hat{\boldsymbol{w}}_j^*\}$ and $\{\breve{\boldsymbol{w}}_k^*\}$, respectively. For example

$$\boldsymbol{e}(n) = \boldsymbol{t}(n) - \boldsymbol{z}(n)$$

$$= \boldsymbol{t}(n) - \sum_{k=1}^{k_2-1} \tilde{\boldsymbol{w}}_k^*(n)\boldsymbol{t}(n-k) - \sum_{j=0}^{k_1-1} \hat{\boldsymbol{w}}_j^*(n)\boldsymbol{y}'(n-j), \tag{3-16}$$

$$\nabla m_1(n) = \frac{\partial \left|\boldsymbol{e}(n)\right|^2}{\partial m_1}$$

$$= \frac{\partial \left[\boldsymbol{e}(n)\boldsymbol{e}^*(n)\right]}{\partial m_1}$$

$$= \frac{\partial \boldsymbol{e}(n)}{\partial m_1}\boldsymbol{e}^*(n) + \frac{\partial \boldsymbol{e}^*(n)}{\partial m_1}\boldsymbol{e}(n), \tag{3-17}$$

$$\frac{\partial \boldsymbol{e}(n)}{\partial m_1} = -\sum_{j=0}^{k_1-1} \hat{\boldsymbol{w}}_j^*(n)\frac{\partial \boldsymbol{y}'(n-j)}{\partial m_1}$$

$$= -\sum_{j=0}^{k_1-1} \hat{\boldsymbol{w}}_j^*(n)x_I(n-j), \tag{3-18}$$

$$\frac{\partial \boldsymbol{e}^*(n)}{\partial m_1} = -\sum_{j=0}^{k_1-1} \hat{\boldsymbol{w}}_j(n)\frac{\partial \boldsymbol{y}'^*(n-j)}{\partial m_1}$$

$$= -\sum_{j=0}^{k_1-1} \hat{\boldsymbol{w}}_j(n)x_I(n-j), \tag{3-19}$$

$$\nabla m_1(n) = -\sum_{j=0}^{k_1-1} \hat{\boldsymbol{w}}_j^*(n)x_I(n-j)\boldsymbol{e}^*(n) - \sum_{j=0}^{k_1-1} \hat{\boldsymbol{w}}_j(n)x_I(n-j)\boldsymbol{e}(n)$$

$$= -2\sum_{j=0}^{k_1-1}\left\{x_I(n-j)\times\left[e_I(n)\times\hat{w}_{jI}(n) - e_Q(n)\times\hat{w}_{jQ}(n)\right]\right\}. \tag{3-20}$$

Here $e_I(n)$ and $e_Q(n)$ denotes the real and imaginary parts of $\boldsymbol{e}(n)$, respectively; $\hat{w}_{jI}(n)$ and $\hat{w}_{jQ}(n)$ denotes the real and imaginary parts of $\hat{\boldsymbol{w}}_j(n)$, respectively. Similarly, it can be obtained that

$$\nabla m_2(n) = -2\sum_{j=0}^{k_1-1}\left\{x_Q(n-j)\times\left[e_I(n)\times\widehat{w}_{jI}(n) - e_Q(n)\times\widehat{w}_{jQ}(n)\right]\right\}, \tag{3-21}$$

$$\nabla m_3(n) = -2\sum_{j=0}^{k_1-1}\left\{x_I(n-j)\times\left[e_I(n)\times\widehat{w}_{jQ}(n) + e_Q(n)\times\widehat{w}_{jI}(n)\right]\right\}, \tag{3-22}$$

$$\nabla m_4(n) = -2\sum_{j=0}^{k_1-1}\left\{x_Q(n-j)\times\left[e_I(n)\times\widehat{w}_{jQ}(n) + e_Q(n)\times\widehat{w}_{jI}(n)\right]\right\}. \tag{3-23}$$

Similarly, we obtain

$$\nabla\overline{\boldsymbol{w}}^*(n) = \frac{\partial\boldsymbol{e}(n)}{\partial\overline{\boldsymbol{w}}^*}\boldsymbol{e}^*(n) + \frac{\partial\boldsymbol{e}^*(n)}{\partial\overline{\boldsymbol{w}}^*}\boldsymbol{e}(n), \tag{3-24}$$

$$\frac{\partial\boldsymbol{e}(n)}{\partial\overline{\boldsymbol{w}}^*} = -\sum_{j=0}^{k_1-1}\widehat{\boldsymbol{w}}_j^*(n)\frac{\partial\left[\boldsymbol{y}(n) + \overline{\boldsymbol{w}}^*(n)\right]}{\partial\overline{\boldsymbol{w}}^*}, \tag{3-25}$$

$$\frac{\partial\boldsymbol{e}^*(n)}{\partial\overline{\boldsymbol{w}}^*} = -\sum_{j=0}^{k_1-1}\widehat{\boldsymbol{w}}_j(n)\frac{\partial\left[\boldsymbol{y}^*(n) + \overline{\boldsymbol{w}}(n)\right]}{\partial\overline{\boldsymbol{w}}^*}. \tag{3-26}$$

According to (6.127) and (6.128) in [11], it can be obtained that:

$$\begin{aligned}\frac{\partial\overline{\boldsymbol{w}}^*(n)}{\partial\overline{\boldsymbol{w}}^*} &= \frac{\partial\overline{\boldsymbol{w}}^*(n)}{\partial\overline{w}_I} - j\frac{\partial\overline{\boldsymbol{w}}^*(n)}{\partial\overline{w}_Q} \\ &= 0,\end{aligned} \tag{3-27}$$

$$\begin{aligned}\frac{\partial\overline{\boldsymbol{w}}(n)}{\partial\overline{\boldsymbol{w}}^*} &= \frac{\partial\overline{\boldsymbol{w}}(n)}{\partial\overline{w}_I} + j\frac{\partial\overline{\boldsymbol{w}}(n)}{\partial\overline{w}_Q} \\ &= 2.\end{aligned} \tag{3-28}$$

Then we get

$$\nabla \bar{\boldsymbol{w}}^*(n) = -2\sum_{j=0}^{k_1-1} \hat{\boldsymbol{w}}_j(n)\boldsymbol{e}(n). \tag{3-29}$$

Similarly $\nabla \hat{\boldsymbol{w}}_j^*(n)$ and $\nabla \breve{\boldsymbol{w}}_k^*(n)$ can be obtained too. But according to the principle of orthogonality [11] [14], it is can be easily obtained that

$$\nabla \hat{\boldsymbol{w}}_j^*(n) = -2\boldsymbol{y}'^*(n-j)\times \boldsymbol{e}(n) \quad (j = 0,1,\cdots,k_1-1), \tag{3-30}$$

$$\nabla \breve{\boldsymbol{w}}_k^*(n) = -2\boldsymbol{t}^*(n-k)\times \boldsymbol{e}(n) \quad (k = 1,2,\cdots,k_2-1). \tag{3-31}$$

3.5 Internal Iterative Algorithm

According to (3-20)-(3-22) and (3-29)-(3-31), it is seen that there are interactions among the adaptations of $\{m_i\}$, $\bar{\boldsymbol{w}}^*$, $\{\hat{\boldsymbol{w}}_j^*\}$ and $\{\breve{\boldsymbol{w}}_k^*\}$. Because of the interactions among the adaptations of the different groups of taps, the proposed algorithm is nonlinear, so the filter may result in biased optimum coefficients for CFFE and I/Q mismatch canceller. In other words, the coefficients of the filters may converge to the local optimum values instead of the global optimum values. The analysis of the issue may be prohibitively complicated and is left as the future work, so in the thesis this issue is not discussed in details. In addition, in practical applications, the I/Q mismatch is not very high, so the

initial values of m_1 and m_4 are set to one and m_2 and m_3 are set to zero. In this condition, the biased optimum coefficients do not have much negative influence. To mitigate the interactions among the adaptations of the different groups of taps, an internal iterative algorithm is proposed in the following [9]. A similar iterative algorithm can be found in [15]. Simulation results show that the mismatch canceller can mitigate I/Q mismatch very well and the internal iterative algorithm can accelerate the convergence dramatically. To simplify the representation, (3-16), (3-20)-(3-23) and (3-29)-(3-31) can be represented by using the general symbolic functions $G(\bullet)$, $H(\bullet)$, $I(\bullet)$, $J(\bullet)$ and $K(\bullet)$ as:

$$\boldsymbol{e}(n) = G\left(\boldsymbol{x}(n-j), m_i(n-j), \overline{\boldsymbol{w}}^*(n-j), \widehat{\boldsymbol{w}}_j^*(n), \breve{\boldsymbol{w}}_k^*(n), \boldsymbol{t}(n-k)\right)$$

$$\left((j=0,1,\cdots,k_1-1),(i=1,\cdots,4),(k=1,2,\cdots,k_2-1)\right), \tag{3-32}$$

$$\nabla m_i(n) = H_i\left(\boldsymbol{x}(n-j), \boldsymbol{e}(n), \widehat{\boldsymbol{w}}_j^*(n)\right)\ \left((i=1,\cdots,4),(j=0,1,\cdots,k_1-1)\right), \tag{3-33}$$

$$\nabla \overline{\boldsymbol{w}}^*(n) = I\left(\widehat{\boldsymbol{w}}_j^*(n), \boldsymbol{e}(n)\right)\ (j=0,1,\cdots,k_1-1), \tag{3-34}$$

$$\nabla \widehat{\boldsymbol{w}}_j^*(n) = J\left(\boldsymbol{x}(n-j), m_i(n-j), \overline{\boldsymbol{w}}^*(n-j), \boldsymbol{e}(n)\right)$$

$$\left((i=1,\cdots,4),(j=0,1,\cdots,k_1-1)\right), \tag{3-35}$$

$$\nabla \breve{\boldsymbol{w}}_k^*(n) = K\left(\boldsymbol{t}(n-k), \boldsymbol{e}(n)\right)\ (k=1,2,\cdots,k_2-1). \tag{3-36}$$

Let $\tilde{N}$ denote the total number of internal iterations. Let $m_i^{(l)}(n)$, $\overline{\boldsymbol{w}}^{*(l)}(n)$, $\widehat{\boldsymbol{w}}_j^{*(l)}(n)$, $\breve{\boldsymbol{w}}_k^{*(l)}(n)$ and $\boldsymbol{e}^{(l)}(n)$ denote the updated values of $m_i(n)$, $\overline{\boldsymbol{w}}^*(n)$, $\widehat{\boldsymbol{w}}_j^*(n)$, $\breve{\boldsymbol{w}}_k^*(n)$

and $\boldsymbol{e}(n)$, respectively, after l $\left(l=0,1,\cdots,\tilde{N}-1\right)$ internal iterations at time n. The same notation is applicable to other variables. To reduce the complexity of the algorithm, $m_i(n-j)$ and $\bar{\boldsymbol{w}}^*(n-j)$ $\left(j=1,2,\cdots,k_1-1\right)$ do not take part in the internal iterations at time n, so they are dropped in $G(\bullet)$ and $J(\bullet)$ and only $m_i(n)$ and $\bar{\boldsymbol{w}}^*(n)$ are updated in the internal iterations at time n. Simulation results show that whether $m_i(n-j)$ and $\bar{\boldsymbol{w}}^*(n-j)$ $\left(j=1,2,\cdots,k_1-1\right)$ take part or not in the internal iterations makes little difference in the performance. Then for an arbitrary time n, the initial values of $\{m_i\}$, $\bar{\boldsymbol{w}}^*$, $\left\{\hat{\boldsymbol{w}}_j^*\right\}$ and $\left\{\breve{\boldsymbol{w}}_k^*\right\}$ are given as

$$m_i^{(0)}(n)=m_i(n)\quad\left(i=1,\cdots,4\right), \tag{3-37}$$

$$\bar{\boldsymbol{w}}^{*(0)}(n)=\bar{\boldsymbol{w}}^*(n), \tag{3-38}$$

$$\hat{\boldsymbol{w}}_j^{*(0)}(n)=\hat{\boldsymbol{w}}_j^*(n)\quad\left(j=0,1,\cdots,k_1-1\right), \tag{3-39}$$

$$\breve{\boldsymbol{w}}_k^{*(0)}(n)=\breve{\boldsymbol{w}}_k^*(n)\quad\left(k=1,2,\cdots,k_2-1\right), \tag{3-40}$$

$$\boldsymbol{e}^{(0)}(n)=G\left(\boldsymbol{x}(n-j),m_i^{(0)}(n),\bar{\boldsymbol{w}}^{*(0)}(n),\hat{\boldsymbol{w}}_j^{*(0)}(n),\breve{\boldsymbol{w}}_k^{*(0)}(n)\right). \tag{3-41}$$

Hence the internal iterations can be continued as below.

For $l=0,1,\cdots,\tilde{N}-1$

$$\nabla m_i^{(l)}(n)=H_i\left(\boldsymbol{x}(n-j),\boldsymbol{e}^{(l)}(n),\hat{\boldsymbol{w}}_j^{*(l)}(n)\right),$$

$$m_i^{(l+1)}(n) = m_i^{(l)}(n) + \mu_m \times \nabla m_i^{(l)}(n); \tag{3-42}$$

$$\nabla \bar{\boldsymbol{w}}^{*(l)}(n) = I\left(\hat{\boldsymbol{w}}_j^{*(l)}(n), \boldsymbol{e}^{(l)}(n)\right),$$

$$\bar{\boldsymbol{w}}^{*(l+1)}(n) = \bar{\boldsymbol{w}}^{*(l)}(n) + \mu_d \times \nabla \bar{\boldsymbol{w}}^{*(l)}(n); \tag{3-43}$$

$$\nabla \hat{\boldsymbol{w}}_j^{*(l+1)}(n) = J\left(\boldsymbol{x}(n-j), m_i^{(l)}(n), \bar{\boldsymbol{w}}^{*(l)}(n), \boldsymbol{e}^{(l)}(n)\right),$$

$$\hat{\boldsymbol{w}}_j^{*(l+1)}(n) = \hat{\boldsymbol{w}}_j^{*(l)}(n) + \mu_f \times \nabla \hat{\boldsymbol{w}}_j^{*(l)}(n); \tag{3-44}$$

$$\nabla \breve{\boldsymbol{w}}_k^{*(l)}(n) = K\left(\boldsymbol{t}(n-k), \boldsymbol{e}^{(l)}(n)\right),$$

$$\breve{\boldsymbol{w}}_k^{*(l+1)}(n+1) = \breve{\boldsymbol{w}}_k^{*(l)}(n) + \mu_b \times \nabla \breve{\boldsymbol{w}}_k^{*(l)}(n); \tag{3-45}$$

$$\boldsymbol{e}^{(l+1)}(n) = G\left(\boldsymbol{x}(n-j), m_i^{(l+1)}(n), \bar{\boldsymbol{w}}^{*(l+1)}(n), \hat{\boldsymbol{w}}_j^{*(l+1)}(n), \breve{\boldsymbol{w}}_k^{*(l+1)}(n)\right). \tag{3-46}$$

End

At time $n+1$, the initial tap values are the latest updated tap values at time n, i.e.

$$m_i^{(0)}(n+1) = m_i^{(\tilde{N}-1)}(n), \tag{3-47}$$

$$\bar{\boldsymbol{w}}^{*(0)}(n+1) = \bar{\boldsymbol{w}}^{*(\tilde{N}-1)}(n), \tag{3-48}$$

$$\hat{\boldsymbol{w}}_j^{*(0)}(n+1) = \hat{\boldsymbol{w}}_j^{*(\tilde{N}-1)}(n), \tag{3-49}$$

$$\breve{\boldsymbol{w}}_k^{*(0)}(n+1) = \breve{\boldsymbol{w}}_k^{*(\tilde{N}-1)}(n). \tag{3-50}$$

The next internal iteration goes so forth. After all the taps converge to their optimum values, the training sequence $\boldsymbol{t}(n)$ is replaced by the estimated sequence $\hat{\boldsymbol{t}}(n)$.

3.6 Implementation Complexity

As we know, the eminent feature of the LMS algorithm is its simplicity. The algorithm proposed in the thesis is based on the LMS algorithm and has a simple implementation. There are 4 multiplications for computing $\boldsymbol{y}(n)$, as shown in Fig. 3-1, $1+k_1+k_2$ multiplications for computing output signal $\boldsymbol{z}(n)$, 12 multiplications for updating $\{m_i\}$, 1 multiplication for updating $\bar{\boldsymbol{w}}^*$, $1+k_1$ multiplications for updating $\{\hat{\boldsymbol{w}}_j^*\}$, $1+k_2$ multiplications for updating $\{\breve{\boldsymbol{w}}_k^*\}$, so generally there are $20+2(k_1+k_2)$ multiplications per iteration. Considering the internal iteration, there are $(\tilde{N}+1)[20+2(k_1+k_2)]$ multiplications per iteration involved in the implementation.

3.7 Summary

In this chapter, the structure of the adaptive filters and the adaptive algorithm are given. According to the received signal model in Chapter 2, an I/Q mismatch canceller is employed first to cancel the I/Q mismatch in the received signal. In the thesis, the output of the mismatch canceller $\boldsymbol{y}(n)$ is treated as a complex valued signal with the signal in I channel as its real part and signal in Q channel as its imaginary part. Hence the DC offsets can be cancelled by a complex valued tap $\bar{\boldsymbol{w}}^*$ with 1 as the input. Since the

flicker noise $\boldsymbol{f}(n)$ is modeled as an AR random process, the transmitted signal $\boldsymbol{t}(n)$ can be recovered by filtering $\boldsymbol{y}'(n)$ with a CFFE and a CDFE in sequence. The detailed derivations of the adaptive algorithm are given in Section 3.4. The proposed algorithm is based on LMS algorithm. Due to the interactions among the adaptations of the taps $\{m_i\}$, $\bar{\boldsymbol{w}}^*$, $\{\hat{\boldsymbol{w}}_j^*\}$ and $\{\breve{\boldsymbol{w}}_k^*\}$, an internal iterative algorithm is introduced in Section 3.5 to mitigate the interactions and to accelerate the convergence of the algorithm. In addition, the implementation complexity of the algorithm is discussed in terms of multiplication in Section 3.6. It should be noted that because the interactions among the adaptations of the different groups of taps, the proposed algorithm is nonlinear, so the filter may result in biased optimum coefficients for CFFE and I/Q mismatch canceller. The analysis of the issue may be prohibitively complicated and is left as the future work, so in the thesis this issue is not discussed in details. In addition, in practical applications, the I/Q mismatch is not very high, so the initial values of m_1 and m_4 are set to one and m_2 and m_3 are set to zero. In this condition, the biased optimum coefficients do not have much negative influence. Simulation results in Chapter 5 show that the mismatch canceller can mitigate I/Q mismatch very well and the internal iterative algorithm can accelerate the convergence dramatically.

CHAPTER 4

CONVERGENCE ANALYSIS

4.1 Outline

In this chapter, the convergence analysis of the proposed algorithm is given in Section 4.2. Due to the complicated structure of the filters, in the thesis only the convergence in the mean of the taps is discussed.

4.2 Convergence Analysis

As described in Chapter 3, the proposed algorithm is based on LMS algorithm, and the adaptive filters are composed of several concatenated adaptive filters. As a result, there are four step sizes involved in the taps' adaptations. Consequently the stability analysis of the algorithm is very important. Because the structure of the proposed adaptive filters is very complicated, it is difficult to derive the convergence of the variances of the elements of the taps to some limited values. In this section, only the convergence of the mean of the taps is discussed. As we know, the independent assumption is based on the assumption that the step size is very small, thus the results obtained based on the independent assumption are also questionable. But the aim of this section is that based on the results derived, we can find the step sizes within the requirements to guarantee the convergence of the algorithm accordingly.

Denote

$$\widehat{W}(n)=\left[\widehat{\boldsymbol{w}}_0^*(n) \quad \widehat{\boldsymbol{w}}_1^*(n) \quad \cdots \quad \widehat{\boldsymbol{w}}_{N_a-1}^*(n)\right]^H, \tag{4-1}$$

$$\breve{W}(n)=\left[\breve{\boldsymbol{w}}_1^*(n) \quad \breve{\boldsymbol{w}}_2^*(n) \quad \cdots \quad \breve{\boldsymbol{w}}_{N_b-1}^*(n)\right]^H, \tag{4-2}$$

$$Y'(n)=\left[\boldsymbol{y}'^*(n) \quad \boldsymbol{y}'^*(n-1) \quad \ldots \quad \boldsymbol{y}'^*(n-N_a+1)\right]^H, \tag{4-3}$$

$$T'(n)=\left[\boldsymbol{t}^*(n-1) \quad \boldsymbol{t}^*(n-2) \quad \ldots \quad \boldsymbol{t}^*(n-N_b+1)\right]^H. \tag{4-4}$$

In the thesis, the upper case letters represent vectors and the bold upper case letters represent matrices. The superscripts "H" and "T" denote Hermitian and transpose respectively. During training period, according to (3-10), $\boldsymbol{z}(n)$ can be written as

$$\begin{aligned}\boldsymbol{z}(n)&=\widehat{W}^H(n)Y'(n)+\breve{W}^H(n)T'(n)\\&=\left[\widehat{W}^H(n) \quad \breve{W}^H(n)\right]\begin{bmatrix}Y'(n)\\T'(n)\end{bmatrix}.\end{aligned} \tag{4-5}$$

Denote

$$\hat{\boldsymbol{R}}(n)=\begin{bmatrix}Y'(n)\\T'(n)\end{bmatrix}\left[Y'^H(n) \quad T'^H(n)\right], \tag{4-6}$$

$$\boldsymbol{R}=E\left[\hat{\boldsymbol{R}}(n)\right]. \tag{4-7}$$

It should be noted that $\boldsymbol{R}$ is a function of $\{m_i\}\ (i=1,\cdots,4)$ and $\bar{\boldsymbol{w}}^*$ because of $Y'(n)$, and $\{m_i\}\ (i=1,\cdots,4)$ and $\bar{\boldsymbol{w}}^*$ are adjusted according to the algorithm in Chapter 3. Assume λ_{max} is the maximum eigenvalue of $\boldsymbol{R}$. When $\{m_i\}\ (i=1,\cdots,4)$ and $\bar{\boldsymbol{w}}^*$ are kept fixed, $\boldsymbol{y}'(n)$ can be regarded as a kind of channel response of input $\boldsymbol{x}(n)$ and 1. So when only considering CFFE and CDFE, according to Section 6.2 in [11], it is easy to obtain that CFFE and CDFE converge in the mean only when μ_f and μ_b meet the following requirements.

$$0 < \mu_f < 1/\lambda_{max}, \tag{4-8}$$

$$0 < \mu_b < 1/\lambda_{max}. \tag{4-9}$$

(4-8) and (4-9) guarantee the convergence of CFFE and CDFE. When $\hat{W}^H(n)$ and $\breve{W}^H(n)$ are adapted to two sets of values $\hat{W}_c^H$ and $\breve{W}_c^H$ (not necessarily the optimum convergence values), respectively, the algorithm will converge when $\{m_i\}\ (i=1,\cdots,4)$ and $\bar{\boldsymbol{w}}^*$ converge. In the following convergence analysis of $\{m_i\}\ (i=1,\cdots,4)$ and $\bar{\boldsymbol{w}}^*$, $\hat{W}^H(n)$ and $\breve{W}^H(n)$ are regarded as constant values $\hat{W}_c^H$ and $\breve{W}_c^H$, respectively. The convergence requirements of $\{m_i\}\ (i=1,\cdots,4)$ and $\bar{\boldsymbol{w}}^*$ are given in the following paragraphs.

Denote

$$\boldsymbol{e}(n)=\boldsymbol{t}(n)-\boldsymbol{z}(n)$$

$$=\boldsymbol{t}(n)-\begin{bmatrix}\widehat{W}^H(n) & \breve{W}^H(n)\end{bmatrix}\begin{bmatrix}Y'(n)\\ T'(n)\end{bmatrix}$$

$$=\boldsymbol{t}(n)-\begin{bmatrix}\widehat{W}_c^H & \breve{W}_c^H\end{bmatrix}\begin{bmatrix}Y'(n)\\ T'(n)\end{bmatrix}. \tag{4-10}$$

$$\hat{P}(n)=\begin{pmatrix}Y'(n)\boldsymbol{t}^*(n)\\ T'(n)\boldsymbol{t}^*(n)\end{pmatrix}, \tag{4-11}$$

Here (4-10) is obtained based on the assumption that $\widehat{W}^H(n)$ and $\breve{W}^H(n)$ have been adapted to two sets of values $\widehat{W}_c^H$ and $\breve{W}_c^H$. From (3-4)-(3-6) in Chapter 3, it can be obtained that

$$\boldsymbol{y}'(n)=\left[m_1(n)\times x_I(n)+m_2(n)\times x_Q(n)\right]+j\left[m_3(n)\times x_I(n)+m_4(n)\times x_Q(n)\right]+\bar{\boldsymbol{w}}^*(n)$$

$$=\left[m_1(n)+jm_3(n)\right]x_I(n)+\left[m_2(n)+jm_4(n)\right]x_Q(n)+\bar{\boldsymbol{w}}^*(n), \tag{4-12}$$

$$\boldsymbol{y}'(n-k)=\left[m_1(n-k)+jm_3(n-k)\right]x_I(n-k)$$

$$+\left[m_2(n-k)+jm_4(n-k)\right]x_Q(n-k)+\bar{\boldsymbol{w}}^*(n-k). \tag{4-13}$$

The inputs of CFFE at time n are $\boldsymbol{y}'(n-k)$ $(k=0,1,\cdots,k_1-1)$. To simply the derivation, the input of CFFE at time n and $n+1$ can be assumed as

$$\boldsymbol{y}'(n-k)=\left[m_1(n)+jm_3(n)\right]x_I(n-k)+\left[m_2(n)+jm_4(n)\right]x_Q(n-k)+\bar{\boldsymbol{w}}^*(n-k). \quad (4\text{-}14)$$

$$\boldsymbol{y}'(n+1-k)=\left[m_1(n+1)+jm_3(n+1)\right]x_I(n+1-k)$$
$$+\left[m_2(n+1)+jm_4(n+1)\right]x_Q(n+1-k)+\bar{\boldsymbol{w}}^*(n+1-k). \quad (4\text{-}15)$$

Because the step size μ_m is very small, the changes in $\{m_i\}\ (i=1,\cdots,4)$ are small especially when they are near convergence. So this assumption is reasonable in convergence analysis.

Denote

$$\bar{W}(n)=\left[\bar{\boldsymbol{w}}^*(n)\quad \bar{\boldsymbol{w}}^*(n-1)\quad \cdots\quad \bar{\boldsymbol{w}}^*(n-N_a+1)\right]^T, \quad (4\text{-}16)$$

$$X_I(n)=\left[x_I(n)\quad x_I(n-1)\quad \ldots\quad x_I(n-N_a+1)\right]^T, \quad (4\text{-}17)$$

$$X_Q(n)=\left[x_Q(n)\quad x_Q(n-1)\quad \ldots\quad x_Q(n-N_a+1)\right]^T. \quad (4\text{-}18)$$

It can be obtained that

$$\hat{P}(n)=\begin{pmatrix}\left\{\left[m_1(n)+jm_3(n)\right]X_I(n)+\left[m_2(n)+jm_4(n)\right]X_Q(n)+\bar{W}(n)\right\}\boldsymbol{t}^*(n)\\ T'(n)\boldsymbol{t}^*(n)\end{pmatrix}. \quad (4\text{-}19)$$

The square error is

$$\hat{\xi}(n)=\left|\boldsymbol{e}(n)\right|^2$$

$$=\left|\boldsymbol{t}^2(n)\right|-\begin{pmatrix}\widehat{W}_c\\ \breve{W}_c\end{pmatrix}^H\hat{P}(n)-\hat{P}^H(n)\begin{pmatrix}\widehat{W}_c\\ \breve{W}_c\end{pmatrix}+\begin{pmatrix}\widehat{W}_c\\ \breve{W}_c\end{pmatrix}^H\hat{\boldsymbol{R}}(n)\begin{pmatrix}\widehat{W}_c\\ \breve{W}_c\end{pmatrix}. \tag{4-20}$$

Then

$$\frac{\partial\hat{\xi}(n)}{\partial m_1}=-\begin{pmatrix}\widehat{W}_c\\ \breve{W}_c\end{pmatrix}^H\frac{\partial\hat{P}(n)}{\partial m_1}-\frac{\partial\hat{P}^H(n)}{\partial m_1}\begin{pmatrix}\widehat{W}_c\\ \breve{W}_c\end{pmatrix}+\begin{pmatrix}\widehat{W}_c\\ \breve{W}_c\end{pmatrix}^H\frac{\partial\hat{\boldsymbol{R}}(n)}{\partial m_1}\begin{pmatrix}\widehat{W}_c\\ \breve{W}_c\end{pmatrix}. \tag{4-21}$$

According to (4-19), it can be obtained

$$\frac{\partial\hat{P}(n)}{\partial m_1}=\begin{pmatrix}X_I(n)\boldsymbol{t}^*(n)\\ \boldsymbol{0}_{(N_b-1)\times 1}\end{pmatrix}. \tag{4-22}$$

$$\frac{\partial\hat{P}^H(n)}{\partial m_1}=\begin{pmatrix}\boldsymbol{t}^T(n)X_I^T(n) & \boldsymbol{0}_{1\times(N_b-1)}\end{pmatrix}. \tag{4-23}$$

In the thesis $\boldsymbol{0}_{m\times n}$ denotes a $m\times n$ null matrix. From (3-3)-(3-6), it can be obtained

$$\boldsymbol{y}'(n-k)\boldsymbol{y}'^*(n-l)=\left[\boldsymbol{y}(n-k)+\bar{\boldsymbol{w}}^*(n-k)\right]\left[\boldsymbol{y}^*(n-l)+\bar{\boldsymbol{w}}(n-l)\right]$$

$$=\boldsymbol{y}(n-k)\boldsymbol{y}^*(n-l)+\boldsymbol{y}(n-k)\bar{\boldsymbol{w}}(n-l)$$

$$+\bar{\boldsymbol{w}}^*(n-k)\boldsymbol{y}^*(n-l)+\bar{\boldsymbol{w}}^*(n-k)\bar{\boldsymbol{w}}(n-l). \tag{4-24}$$

Here $(k=0,1,\cdots,k_1-1)$ and $(l=0,1,\cdots,k_1-1)$. From (4-14), it can be obtained

$$\begin{aligned}\boldsymbol{y}(n-k)\boldsymbol{y}^*(n-l)&=\left\{\left[m_1(n)+jm_3(n)\right]x_I(n-k)+\left[m_2(n)+jm_4(n)\right]x_Q(n-k)\right\}\\&\times\left\{\left[m_1(n)-jm_3(n)\right]\times x_I(n-l)+\left[m_2(n)-jm_4(n)\right]\times x_Q(n-l)\right\}\\&=\left[m_1^2(n)+m_3^2(n)\right]\times\left[x_I(n-k)x_I(n-l)\right]\\&+\left[m_2^2(n)+m_4^2(n)\right]\times\left[x_Q(n-k)x_Q(n-l)\right]\\&+\left[m_1(n)+jm_3(n)\right]\times\left[m_2(n)-jm_4(n)\right]\times\left[x_I(n-k)x_Q(n-l)\right]\\&+\left[m_1(n)-jm_3(n)\right]\times\left[m_2(n)+jm_4(n)\right]\times\left[x_I(n-l)x_Q(n-k)\right].\end{aligned}\tag{4-25}$$

$$\begin{aligned}\frac{\partial\left[\boldsymbol{y}'(n-k)\boldsymbol{y}'^*(n-l)\right]}{\partial m_1}&=\frac{\partial\left[\boldsymbol{y}(n-k)\boldsymbol{y}^*(n-l)\right]}{\partial m_1}+\frac{\partial\left[\boldsymbol{y}(n-k)\bar{\boldsymbol{w}}(n-l)\right]}{\partial m_1}\\&+\frac{\partial\left[\bar{\boldsymbol{w}}^*(n-k)\boldsymbol{y}^*(n-l)\right]}{\partial m_1}+\frac{\partial\left[\bar{\boldsymbol{w}}^*(n-k)\bar{\boldsymbol{w}}(n-l)\right]}{\partial m_1}.\end{aligned}\tag{4-26}$$

From (4-25) it can be obtained

$$\begin{aligned}\frac{\partial\left[\boldsymbol{y}(n-k)\boldsymbol{y}^*(n-l)\right]}{\partial m_1}&=2m_1(n)x_I(n-k)x_I(n-l)\\&+\left[m_2(n)-jm_4(n)\right]\times\left[x_I(n-k)x_Q(n-l)\right]\\&+\left[m_2(n)+jm_4(n)\right]\times\left[x_I(n-l)x_Q(n-k)\right].\end{aligned}\tag{4-27}$$

From (4-14), it can be obtained:

$$\frac{\partial\left[\boldsymbol{y}\left(n-k\right)\bar{\boldsymbol{w}}\left(n-l\right)\right]}{\partial m_1}=x_I\left(n-k\right)\bar{\boldsymbol{w}}\left(n-l\right), \tag{4-28}$$

$$\frac{\partial\left[\bar{\boldsymbol{w}}^*\left(n-k\right)\boldsymbol{y}^*\left(n-l\right)\right]}{\partial m_1}=\bar{\boldsymbol{w}}^*\left(n-k\right)x_I\left(n-l\right), \tag{4-29}$$

$$\frac{\partial\left[\bar{\boldsymbol{w}}^*\left(n-k\right)\bar{\boldsymbol{w}}\left(n-l\right)\right]}{\partial m_1}=0. \tag{4-30}$$

Combining (4-27)-(4-30), it can be obtained

$$\frac{\partial\left[\boldsymbol{y}'\left(n-k\right)\boldsymbol{y}'^*\left(n-l\right)\right]}{\partial m_1}=2m_1\left(n\right)x_I\left(n-k\right)x_I\left(n-l\right)+\hat{m}_{1kl}\left(n\right). \tag{4-31}$$

Here $\hat{m}_{1kl}\left(n\right)\left(k=0,1,\cdots,k_1-1;l=0,1,\cdots,k_1-1\right)$ represents the remaining parts which do not contain $m_1\left(n\right)$.

Denote

$$\hat{\boldsymbol{R}}_{Y'}\left(n\right)=Y'\left(n\right)Y'^H\left(n\right), \tag{4-32}$$

$$\hat{\boldsymbol{R}}_{T'}\left(n\right)=T'\left(n\right)T'^H\left(n\right), \tag{4-33}$$

$$\hat{\boldsymbol{R}}_{XI}\left(n\right)=X_I\left(n\right)X_I^T\left(n\right), \tag{4-34}$$

$$\hat{\boldsymbol{R}}_{XQ}(n) = X_Q(n) X_Q^T(n). \tag{4-35}$$

From (4-31), it can be obtained

$$\frac{\partial \hat{\boldsymbol{R}}_{Y'}(n)}{\partial m_1} = 2m_1(n)\hat{\boldsymbol{R}}_{XI}(n) + \hat{\boldsymbol{M}}_1(n). \tag{4-36}$$

Here $\hat{\boldsymbol{M}}_1(n)$ is the $k_1 \times k_1$ matrix with the elements of $\hat{m}_{1kl}(n)$ $(k = 0,1,\cdots,k_1-1; l = 0,1,\cdots,k_1-1)$. From (4-14) and (4-33), we can obtain

$$\frac{\partial \left[Y'(n) T'^H(n) \right]}{\partial m_1} = X_I(n) T'^H(n), \tag{4-37}$$

$$\frac{\partial \left[T'(n) Y'^H(n) \right]}{\partial m_1} = T'(n) X_I^T(n), \tag{4-38}$$

$$\frac{\partial \hat{\boldsymbol{R}}_{T'}(n)}{\partial m_1} = \boldsymbol{0}_{(N_b-1)\times(N_b-1)}. \tag{4-39}$$

From (4-21)-(4-23) and (4-36)-(4-39), it can be obtained

$$\frac{\partial \hat{\xi}(n)}{\partial m_1} = -\begin{pmatrix} \widehat{W}_c \\ \breve{W}_c \end{pmatrix}^H \begin{pmatrix} X_I(n)\boldsymbol{t}^*(n) \\ \boldsymbol{0}_{(N_b-1)\times 1} \end{pmatrix} - \begin{pmatrix} \boldsymbol{t}^T(n) X_I^T(n) & \boldsymbol{0}_{1\times(N_b-1)} \end{pmatrix} \begin{pmatrix} \widehat{W}_c \\ \breve{W}_c \end{pmatrix}$$

$$+ \begin{pmatrix} \widehat{W}_c \\ \breve{W}_c \end{pmatrix}^H \begin{pmatrix} 2m_1(n)\hat{\boldsymbol{R}}_{XI}(n) + \hat{\boldsymbol{M}}_1(n) & X_I(n) T'^H(n) \\ T'(n) X_I^T(n) & \boldsymbol{0}_{(N_b-1)\times(N_b-1)} \end{pmatrix} \begin{pmatrix} \widehat{W}_c \\ \breve{W}_c \end{pmatrix}$$

$$= -\widehat{W}_c^H X_I(n)\boldsymbol{t}^*(n) - \boldsymbol{t}^T(n) X_I^T(n)\widehat{W}_c$$

$$+\widehat{W}_c^H 2m_1(n)\hat{\boldsymbol{R}}_{XI}(n)\widehat{W}_c + \widehat{W}_c^H \hat{\boldsymbol{M}}_1(n)\widehat{W}_c$$

$$+\breve{W}_c^H T'(n) X_I^T(n)\widehat{W}_c + \widehat{W}_c^H X_I(n) T'^H(n)\breve{W}_c . \qquad (4\text{-}40)$$

According to LMS algorithm, it can be obtained

$$m_1(n+1) = m_1(\mathrm{n}) - \mu_m \frac{\partial \hat{\xi}(n)}{\partial m_1} . \qquad (4\text{-}41)$$

As we know, LMS on average follows the same trajectory as the steepest-descent algorithm [11]. According to Section 6.2 in [11], we can get the convergence requirements of $\{m_i\}$ from the method of steepest descent:

$$E\left[m_1(n+1)\right] = E\left[m_1(\mathrm{n})\right] - \mu_m E\left[\frac{\partial \hat{\xi}(n)}{\partial m_1}\right]$$

$$= E\left[m_1(\mathrm{n})\right] - \mu_m \left\{\widehat{W}_c^H E\left[2m_1(n)\hat{\boldsymbol{R}}_{XI}(n)\right]\widehat{W}_c\right\}$$

$$+\mu_m \left\{\widehat{W}_c^H E\left[X_I(n)\boldsymbol{t}^*(n)\right] + E\left[\boldsymbol{t}^T(n) X_I^T(n)\right]\widehat{W}_c - \widehat{W}_c^H E\left[\hat{\boldsymbol{M}}_1(n)\right]\widehat{W}_c\right\}$$

$$-\mu_m \left\{\breve{W}_c^H E\left[T'(n) X_I^T(n)\right]\widehat{W}_c + \widehat{W}_c^H E\left[X_I(n) T'^H(n)\right]\breve{W}_c\right\} . \qquad (4\text{-}42)$$

Setting $E\left(\frac{\partial \hat{\xi}(n)}{\partial m_1}\right)$ to zero, m_{1o} can be obtained which satisfies the equation

$$\widehat{W}_c^H 2m_{1o} E\left[\hat{\boldsymbol{R}}_{XI}(n)\right]\widehat{W}_c = \widehat{W}_c^H E\left[X_I(n)\boldsymbol{t}^*(n)\right] + E\left[\boldsymbol{t}^T(n) X_I^T(n)\right]\widehat{W}_c$$

$$-\widehat{W}_c^H E\left[\hat{\boldsymbol{M}}_1(n)\right]\widehat{W}_c - \breve{W}_c^H E\left[T'(n) X_I^T(n)\right]\widehat{W}_c$$

$$-\widehat{W}_c^H E\left[X_I(n) T'^H(n)\right]\breve{W}_c . \qquad (4\text{-}43)$$

Denote $v_{m_1}(n) = m_1(n) - m_{1o}$. In the thesis the subscript "o" represents the optimum. It can be obtained from (4-42) and (4-43) that

$$E\left[v_{m_1}(n+1)\right] = E\left[v_{m_1}(n)\right] - 2\mu_m \widehat{W}_c^H E\left[v_{m_1}(n)\hat{\boldsymbol{R}}_{XI}(n)\right]\widehat{W}_c . \qquad (4\text{-}44)$$

By employing the independence assumption (pp.142 in [11]), it can be obtained that

$$E\left[v_{m_1}(n+1)\right] = \left(1 - 2\mu_m \widehat{W}_c^H \boldsymbol{R}_{XI}\widehat{W}_c\right) E\left[v_{m_1}(n)\right]. \qquad (4\text{-}45)$$

Here $\boldsymbol{R}_{XI} = E\left[\hat{\boldsymbol{R}}_{XI}(n)\right]$. Similarly, we can obtain

$$E\left[v_{m_2}(n+1)\right] = \left(1 - 2\mu_m \widehat{W}_c^H \boldsymbol{R}_{XQ}\widehat{W}_c\right) E\left[v_{m_2}(n)\right]. \qquad (4\text{-}46)$$

$$E\left[v_{m_3}(n+1)\right] = \left(1 - 2\mu_m \widehat{W}_c^H \boldsymbol{R}_{XI}\widehat{W}_c\right) E\left[v_{m_3}(n)\right]. \qquad (4\text{-}47)$$

$$E\left[v_{m_4}(n+1)\right]=\left(1-2\mu_m \widehat{W}_c^H \boldsymbol{R}_{XQ} \widehat{W}_c\right) E\left[v_{m_4}(n)\right]. \tag{4-48}$$

Here $\boldsymbol{R}_{XQ}=E\left[\hat{\boldsymbol{R}}_{XQ}(n)\right]$. Consequently $\{m_i\}$ converge when

$$0<\mu_m<\min\left(\left(\widehat{W}_c^H \boldsymbol{R}_{XI} \widehat{W}_c\right)^{-1},\left(\widehat{W}_c^H \boldsymbol{R}_{XQ} \widehat{W}_c\right)^{-1}\right). \tag{4-49}$$

Because the step size μ_d is very small, the change in $\bar{\boldsymbol{w}}^*$ is small too especially when it is near convergence. So $\bar{\boldsymbol{w}}^*(n-k)$ in (4-14) and $\bar{\boldsymbol{w}}^*(n+1-k)$ in (4-15) can be replaced by $\bar{\boldsymbol{w}}^*(n)$ and $\bar{\boldsymbol{w}}^*(n+1)$, respectively. Based on this assumption, the vector in (4-16) can be written as $\bar{\boldsymbol{w}}^*(n)\times \boldsymbol{I}_{N_a\times 1}$. In this thesis $\boldsymbol{I}_{m\times n}$ denotes a $m\times n$ matrix with all elements as 1. By similar derivation, it can be obtained

$$\begin{aligned} E\left[\boldsymbol{v}_{\bar{\boldsymbol{w}}}^*(n+1)\right] &= E\left[\boldsymbol{v}_{\bar{\boldsymbol{w}}}^*(n)\right]-2\mu_d E\left[\boldsymbol{v}_{\bar{\boldsymbol{w}}}^*(n)\right]\widehat{W}^H \boldsymbol{I}_{N_a\times N_a}\widehat{W} \\ &= E\left[\boldsymbol{v}_{\bar{\boldsymbol{w}}}^*(n)\right]\left\{1-2\mu_d\left[\sum_{i=0}^{N_a-1}\widehat{\boldsymbol{w}}_i^*(n)\sum_{i=0}^{N_a-1}\widehat{\boldsymbol{w}}_i(n)\right]\right\}. \end{aligned} \tag{4-50}$$

Here $\boldsymbol{v}_{\bar{\boldsymbol{w}}}(n)=\bar{\boldsymbol{w}}(n)-\bar{\boldsymbol{w}}_o$, $\bar{\boldsymbol{w}}_o$ is obtained by setting $E\left[\dfrac{\partial\hat{\xi}(n)}{\partial\bar{\boldsymbol{w}}^*}\right]$ to zero. Then the convergence condition of DC canceller is

$$0 < \mu_d < \left[\sum_{i=0}^{N_a-1} \widehat{\boldsymbol{w}}_i(n) \sum_{i=0}^{N_a-1} \widehat{\boldsymbol{w}}_i^*(n) \right]^{-1}. \tag{4-51}$$

Because we can always find μ_f, μ_b, μ_m and $\mu_{\bar{w}}$ to satisfy (4-8), (4-9), (4-49) and (4-51) simultaneously, the mean convergence of the algorithm is guaranteed.

4.3 Summary

In this chapter the convergence of the mean of the taps is discussed. The adaptive filters are composed of several concatenated adaptive filters and there are four step sizes involved in the taps' adaptations, so it is difficult to derive the convergence of the variances of the elements of the taps to some limited values. In this chapter, only the convergence of the mean of the taps is discussed and the ranges of the four step sizes to meet the convergence in the mean are derived, respectively. As we know, the requirements of the step sizes obtained based on the independent assumption are questionable. But within the requirements, we can find the step sizes to guarantee the convergence of the algorithm.

CHAPTER 5

SIMULATION RESULTS

5.1 Outline

In this chapter, various simulation results are given to verify the proposed algorithm. In Section 5.3 and Section 5.4, the performances of mismatch canceller and DC offsets canceller, respectively, are given. When I/Q mismatch and DC offsets exist simultaneously, the performance of mismatch canceller and DC offsets canceller is given in Section 5.5. In addition, the performances of CDFE and the internal iterations are given in Section 5.6 and in Section 5.7, respectively. Moreover, the comprehensive performance of the proposed is given in Section 5.8.

5.2 Introduction

The algorithm proposed in this thesis is aimed to simultaneously cancel I/Q mismatch, DC offsets, flicker noise and ISI by complex adaptive filters. In order to verify the performance of each canceller and equalizer respectively, other cancellers or equalizers and distortions should not exist when doing simulations to test the efficiency of one canceller. For example, when doing simulations to verify the efficiency of mismatch canceller, the received signal is only corrupted by I/Q mismatch, ISI and AWGN, and the tap of DC offsets canceller is set to zero, so other distortions and factors such as DC

offsets and flicker noise will not influence the performance of the mismatch canceller; when doing simulations to verify the efficiency of DC offsets canceller, the received signal is only corrupted by DC offsets, ISI and AWGN, m_1 and m_4 of the mismatch canceller are set to one, and m_2 and m_3 are set to zero, so I/Q mismatch and flicker noise will not influence the performance of the DC offsets canceller. In the following sections, the simulation results for these cancellers and equalizers are illustrated and discussed.

5.3 Performance of Mismatch Canceller

To verify the efficiency of the mismatch canceller, the tap of the DC offsets canceller should be set to zero and the received signal to be processed should be only corrupted by ISI, I/Q mismatch and AWGN, so other distortions do not influence its performance. As shown in Fig. 5-1, five curves are illustrated to show the efficiency of the mismatch canceller. In the thesis the signal to noise power ratio (SNR) represents the power ratio of the transmitted signal to AWGN. In the simulations, 16 QAM signals are passed through a channel $H(z)=z+(0.36+0.21j)z^{-1}$ and then corrupted by I/Q mismatch and AWGN. The algorithm parameters are chosen as: $\mu_m=9\times10^{-6}$, $\mu_f=9\times10^{-6}$, $\mu_b=8\times10^{-6}$, $k_1=6$, $k_2=5$, $\tilde{N}=3$. In condition 1, $\alpha=1.5$, $\beta=0.5$, $\phi=10°$, and in condition 2, $\alpha=1.5$, $\beta=0.5$, $\phi=20°$. It is seen that without the mismatch canceller, the bit error rates (BERs) of the two curves are around 10^{-1} , but with the canceller, they decrease

dramatically. Especially in condition 1, the curve is close to the lower bound that is obtained without any mismatch. So the mismatch canceller meets the requirement very well because normally the gain imbalance is $2-3\%$ and the phase imbalance is $2-3°$, which is smaller than that in the condition 1.

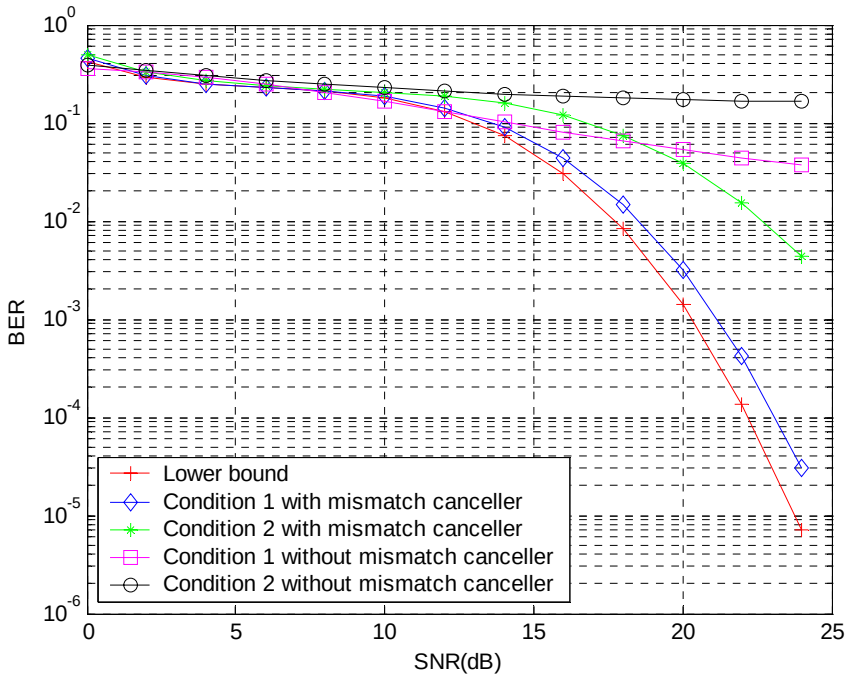

Fig. 5-1 BER performance of the mismatch canceller.

5.4 Performance of DC Offsets Canceller

In the simulations, 16 QAM signals are passed through a channel $H(z)=z+(0.36+0.21j)z^{-1}$ and then corrupted by varying DC offset $\tilde{\boldsymbol{d}}(n)$, constant DC offset $\bar{\boldsymbol{d}}(n)$ and AWGN. Because there is no I/Q mismatch, m_1 and m_4 are set to one

and m_2 and m_3 are set to zero. The varying DC offset $\tilde{\boldsymbol{d}}(n)$ and the transmitted signal have similar energy according to the model in Section 2.3. The other algorithm parameters are chosen as: $\mu_f = 9\times10^{-6}$, $\mu_d = 9\times10^{-3}$, $\mu_b = 8\times10^{-6}$, $k_1 = 6$, $k_2 = 5$, $\tilde{N} = 1$. Four curves are illustrated in Fig. 5-2 to show the performance of the DC offsets canceller. Here SDR represents the power ratio of the desired signal to the constant DC offset $\bar{\boldsymbol{d}}(n)$, and the lower bound is obtained without any DC offsets. As shown in Fig. 5-2, the three BER curves of different SDR are very close to each another, robust to the DC offsets especially when SNR is less than 20 dB. Furthermore, the algorithm performance only degrades 2 dB compared to the lower bound when BER is around 10^{-5} and SDR=30dB, indicating that the canceller can successfully cancel the DC offsets very well.

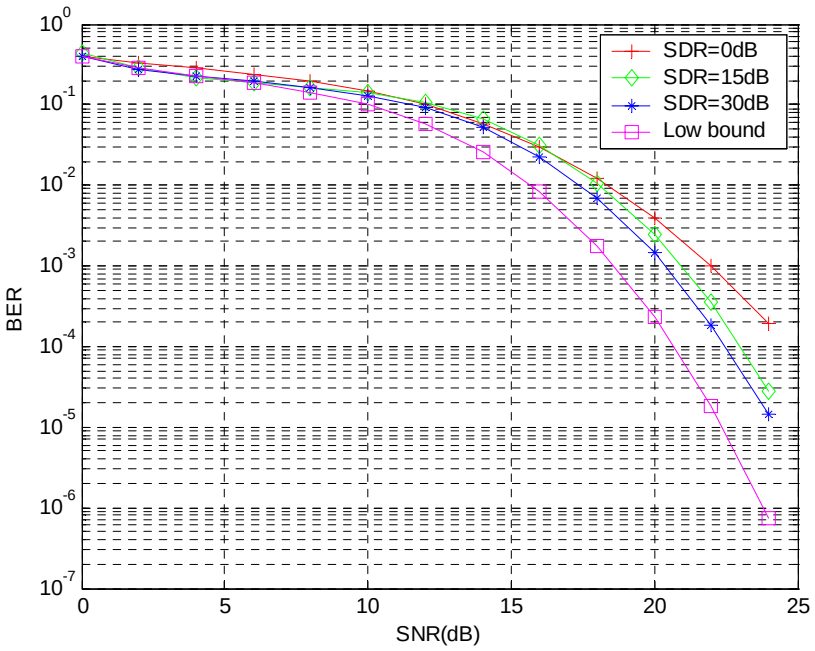

Fig. 5-2 BER performance of the DC offsets canceller.

5.5 Performance of Mismatch Canceller and DC Offsets Canceller

Comprehensive simulation results are given to show the performance of the proposed algorithm when both I/Q mismatch and DC offsets distortions exist. In the simulations, the algorithm parameters are chosen as: $\alpha = 1.2$, $\beta = 0.8$, $\phi = 5°$, $\mu_m = 9\times10^{-6}$, $\mu_f = 9\times10^{-6}$, $\mu_d = 9\times10^{-2}$, $\mu_b = 8\times10^{-6}$, $k_1 = 6$, $k_2 = 5$, $\tilde{N} = 5$. BPSK, QPSK and 16 QAM signals are passed through a channel $H(z) = z + (0.36 + 0.21j)z^{-1}$ and then are corrupted by I/Q mismatch, DC offsets and AWGN, as modeled in Chapter 2. All the taps converge within 10^3 times of adaptations. The BER performance of the proposed algorithm at different SNR and SDR is shown in Fig. 5-3 – Fig. 5-5. Here SDR represents the power ratio of the desired signal to the time varying DC offset $\tilde{\boldsymbol{d}}(n)$ and constant DC offset $\bar{\boldsymbol{d}}(n)$. The varying DC offset $\tilde{\boldsymbol{d}}(n)$ and the transmitted signal have similar energy according to the model in Section 2.3. The SNR varies from 0 to 25 dB and SDR takes values -3, 3 and 6 dB. In addition, the lower bound curves are obtained when transmitted signals are only corrupted by ISI and AWGN. As shown in Fig. 5-3 – Fig. 5-5, the three BER curves for different SDR in each figure are close to each other and robust to DC offsets. Furthermore, even for 16 QAM shown in Fig. 5-5, the algorithm performance only degrades by 2 dB with respect to the lower bound when BER=10^{-5} and SDR= 6 dB, indicating that the adaptive filter can successfully cancel the comprehensive distortions generated by mismatch, DC offsets and ISI.

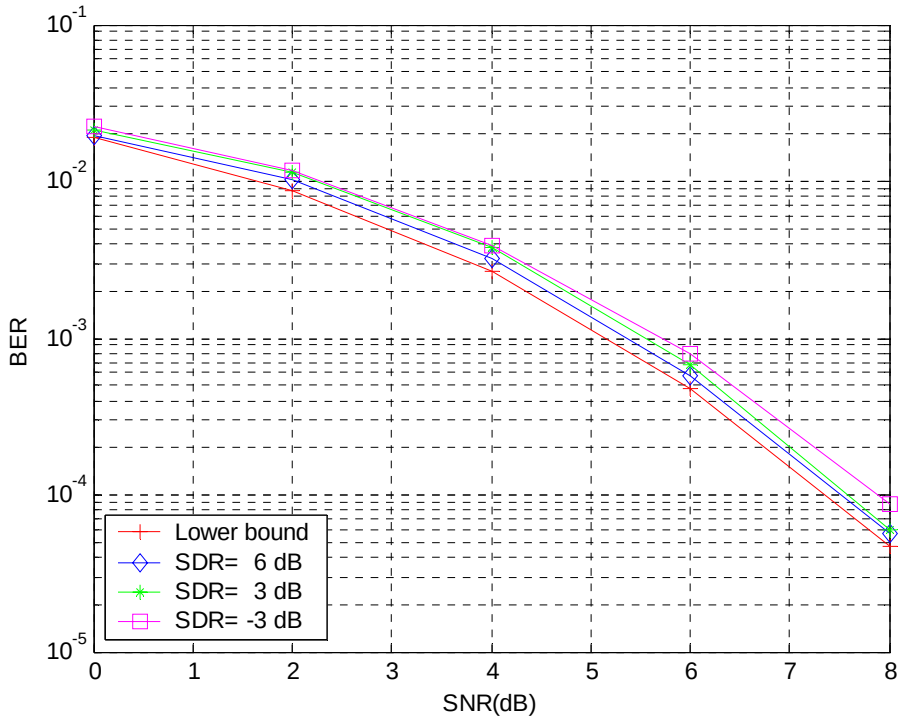

Fig. 5-3 BER performance of BPSK

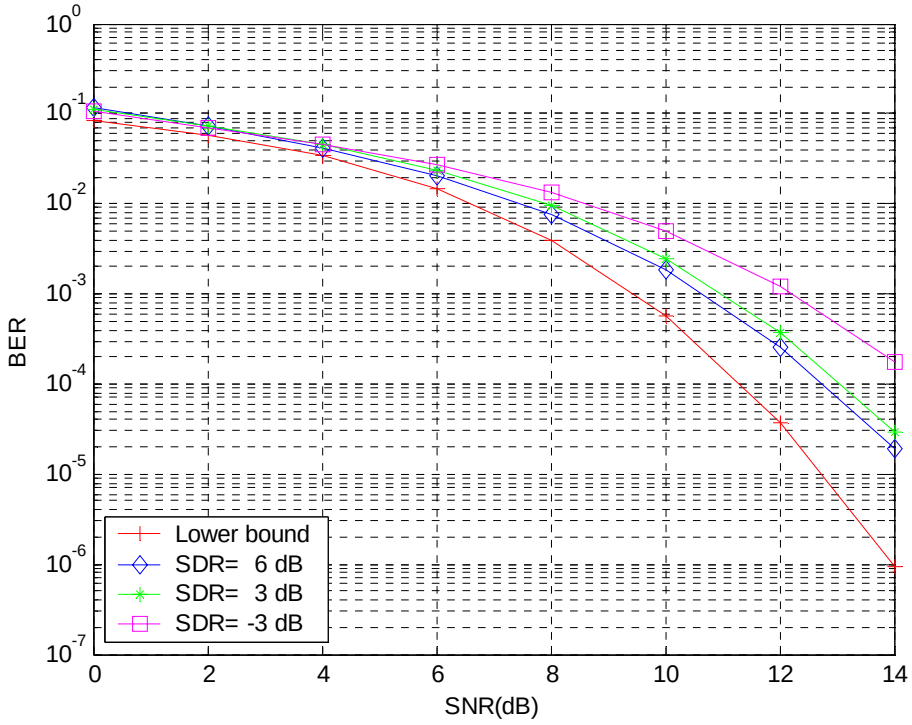

Fig. 5-4 BER performance of QPSK

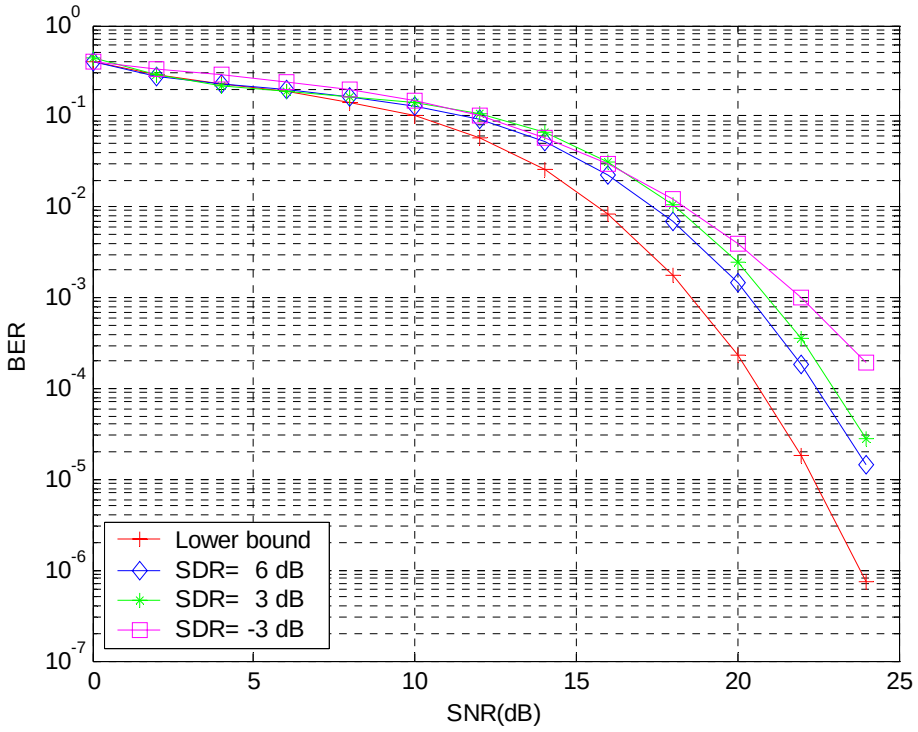

Fig. 5-5 BER performance of 16 QAM

5.6 Performance of CDFE

As shown in Fig. 1-5 in Chapter 1, the PSD of the flicker noise is inversely proportional to frequency. Because in this thesis, the flicker noise is modeled as an AR process and the algorithm is proposed according to this model, and the proposed algorithm can mitigate any noise modeled as AR process, so in the simulations, a low pass Butterworth filter is introduced to generate the colored flicker noise. The orders of the numerator and denominator coefficients of the filter are 0 and 4, respectively. The PSD of the generated flicker noise is shown in Fig. 5-6. In the simulation, the sampling frequency is 512 Hz.

Fig. 5-7 is obtained when QPSK signals are passed through a channel $H(z)=z+(0.36+0.21j)z^{-1}$. In the simulation, the flicker noise is generated by passing a white noise through the low pass Butterworth filter mentioned above. The power ratio of the signal to the flicker noise is 0 dB. So the power of the flicker noise is much higher than the one in practice. It is seen in Fig. 5-7 that when only flicker noise and ISI exist, by only employing the CFFE, the BER is around 10^{-1}. But after employing the CDFE, the BER reaches 10^{-4} at SNR$=20$ dB. So it is obvious that based on the signal model in Chapter 2, CFFE and CDFE can mitigate the flicker noise and ISI efficiently. When ISI, flicker noise, mismatch ($\alpha=1.2$, $\beta=0.8$, $\phi=10°$), varying DC offsets with the similar energy of the transmitted signal and constant DC offsets (SDR=15 dB) exist simultaneously and the internal iteration number takes 6, the BER reaches 10^{-4} at SNR$=26$ dB. Here SDR represents the power ratio of the desired signal to the constant DC offset $\bar{\boldsymbol{d}}(n)$.

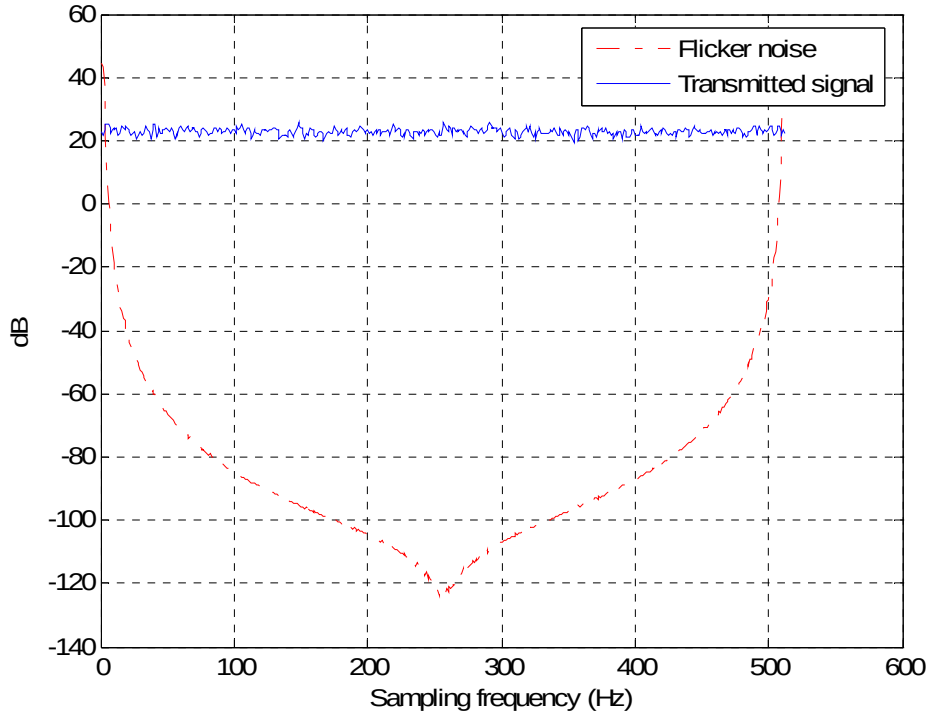

Fig. 5-6 PSD of flicker noise and transmitted signal.

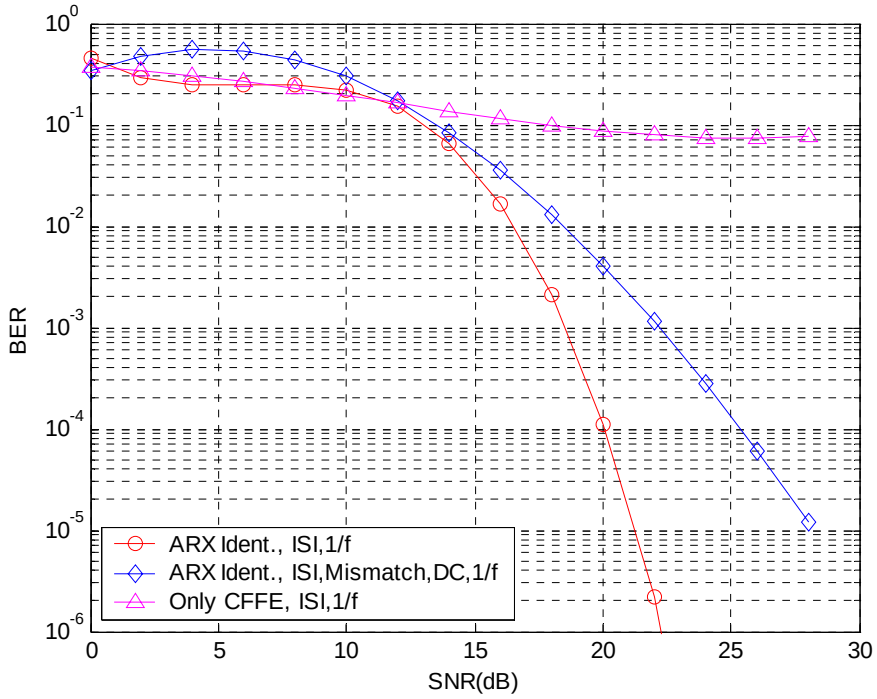

Fig. 5-7 BER performance of CDFE.

5.7 Performance of the Internal Iterations

In Section 3.5 an internal iterative algorithm is introduced to accelerate the convergence of the algorithm and to mitigate the interactions among the adaptations of $\{m_i\}$, $\bar{\boldsymbol{w}}$, $\{\hat{\boldsymbol{w}}_j\}$ and $\{\check{\boldsymbol{w}}_k\}$. Simulations are done to demonstrate the performance enhancement of the internal iterative algorithm. In the simulations, QPSK signals are corrupted by ISI, I/Q mismatch, DC offsets, flicker noise and AWGN as modeled in Chapter 2. The algorithm parameters are chosen as: $\alpha = 1.05$, $\beta = 0.95$, $\phi = 5°$, $\mu_m = 8\times10^{-6}$, $\mu_f = 3\times10^{-6}$, $\mu_d = 1\times10^{-4}$, $\mu_b = 3\times10^{-6}$, $k_1 = 6$, $k_2 = 5$, SFR = 10 dB and SDR=10 dB. Here SFR represents the power ratio of the desired signal to the flicker noise and SDR represents the power ratio of the desired signal to the constant DC offset $\bar{\boldsymbol{d}}(n)$. Flicker noise is generated by passing white noise through a low pass Butterworth filter. The orders of the numerator and denominator coefficients of the filter are 0 and 2, respectively. In the simulations the transmitted signal is corrupted by the varying DC offsets with the similar energy of the transmitted signal and the constant DC offsets. The internal iterative number $\tilde{N} = 6$. The learning curve of the algorithm is obtained by an ensemble average of the sequence $|e(n)|^2$ over 100 independent runs. As shown is Fig. 5-8, the learning curve with internal iterations converges much faster than that without internal iterations does.

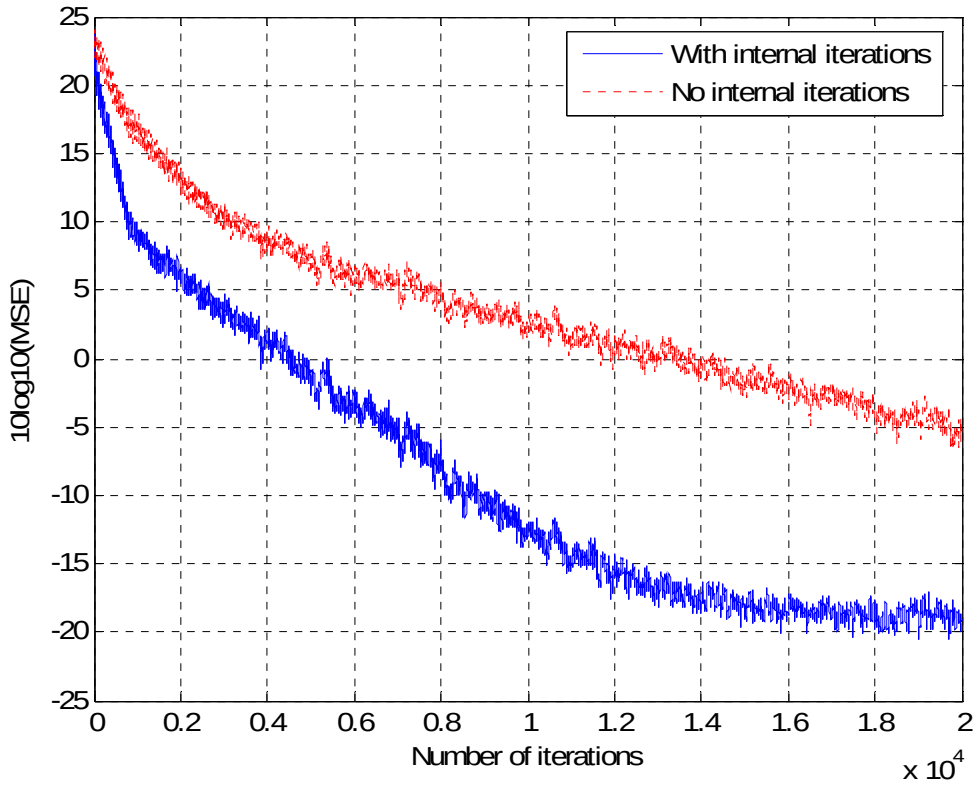

Fig. 5-8 Learning curve of the proposed algorithm without and with internal iterations.

5.8 Comprehensive Performance of the Proposed Algorithm

In this section, comprehensive simulation results are given when BPSK, QPSK and 16QAM signals are passed through a channel $H(z)=z+(0.36+0.21j)z^{-1}$ and are corrupted by all the distortions such as I/Q mismatch, DC offsets, flicker noise and AWGN. As shown in Fig. 5-9 – Fig. 5-11, the lower bound is obtained when the transmitted signal is only corrupted by ISI and AWGN. The algorithm parameters are chosen as: $\mu_m=9\times10^{-6}$, $\mu_f=3\times10^{-6}$, $\mu_d=1\times10^{-2}$, $\mu_b=3\times10^{-6}$, $k_1=6$, $k_2=5$, $\tilde{N}=6$, SDR $=10$ dB. SDR

represents the power ratio of the desired signal to the constant DC offset $\bar{\boldsymbol{d}}(n)$. The varying DC offset $\tilde{\boldsymbol{d}}(n)$ and the transmitted signal have similar energy according to the model in Section 2.3. The flicker noise is generated the same as in Section 5.7, but its power is changed accordingly. In condition 1, $\alpha = 1.05$, $\beta = 0.95$, $\phi = 5°$, and SFR=20 dB. Here SFR represents the power ratio of the desired signal to the flicker noise. In condition 2, $\alpha = 1.05$, $\beta = 0.95$, $\phi = 5°$, and SFR=10 dB. In condition 3, $\alpha = 1.1$, $\beta = 0.9$, $\phi = 10°$, and SFR=10 dB. As shown in Fig. 5-9 – Fig. 5-11, the BER curves of the three conditions are close to one another, robust to mismatch and flicker noise. It is also seen that when BPSK and QPSK signals are transmitted, the BER curves of the three conditions are close to the lower bound too, which indicates that the proposed algorithm can remove all the distortions including ISI very well.

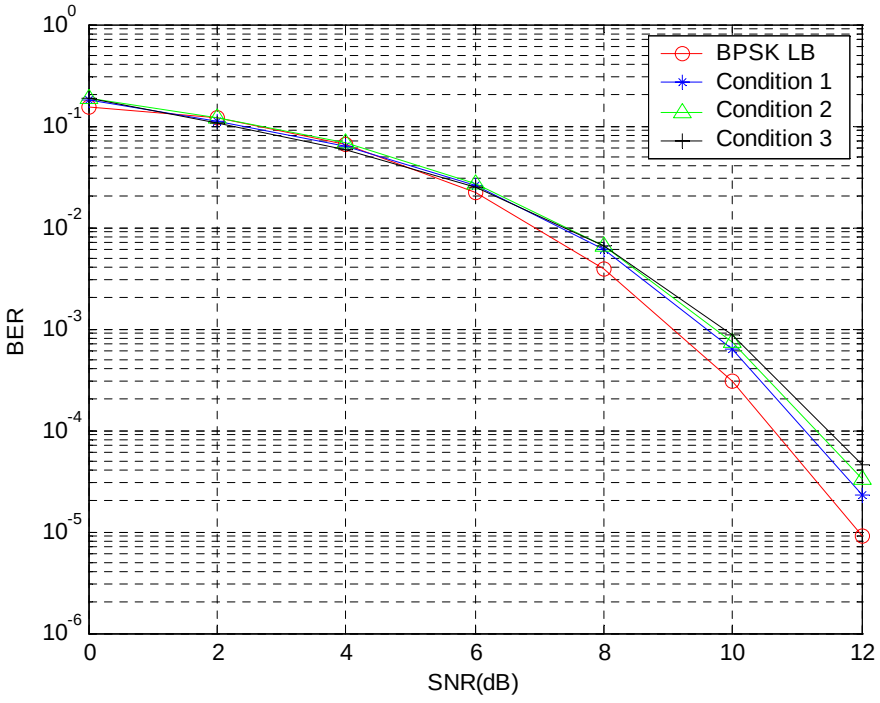

Fig. 5-9 Comprehensive BER performance of BPSK.

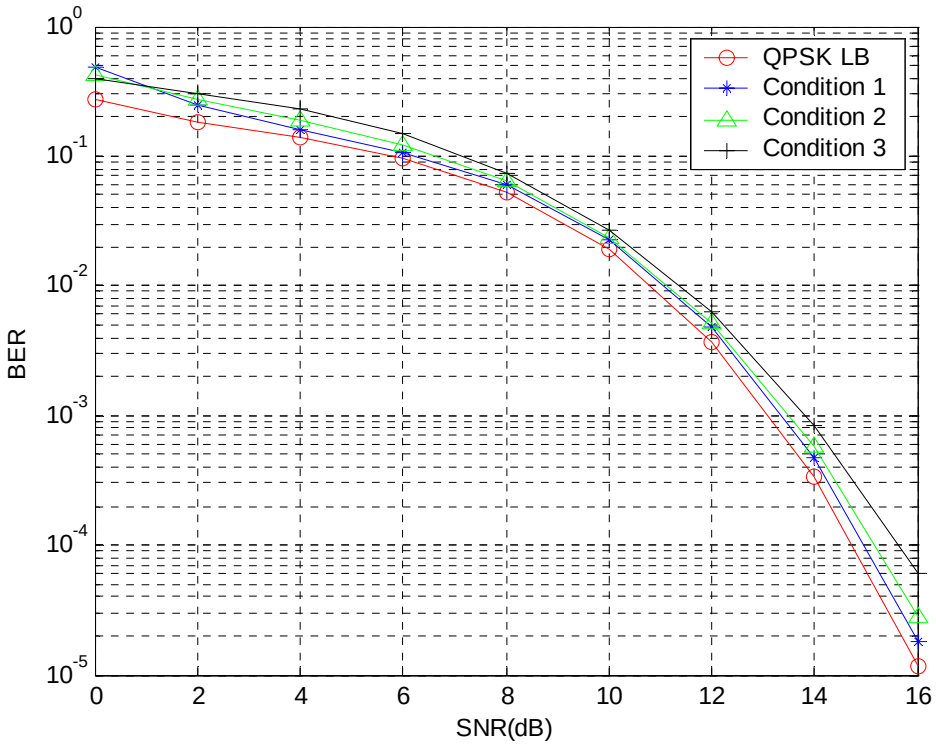

Fig. 5-10 Comprehensive BER performance of QPSK.

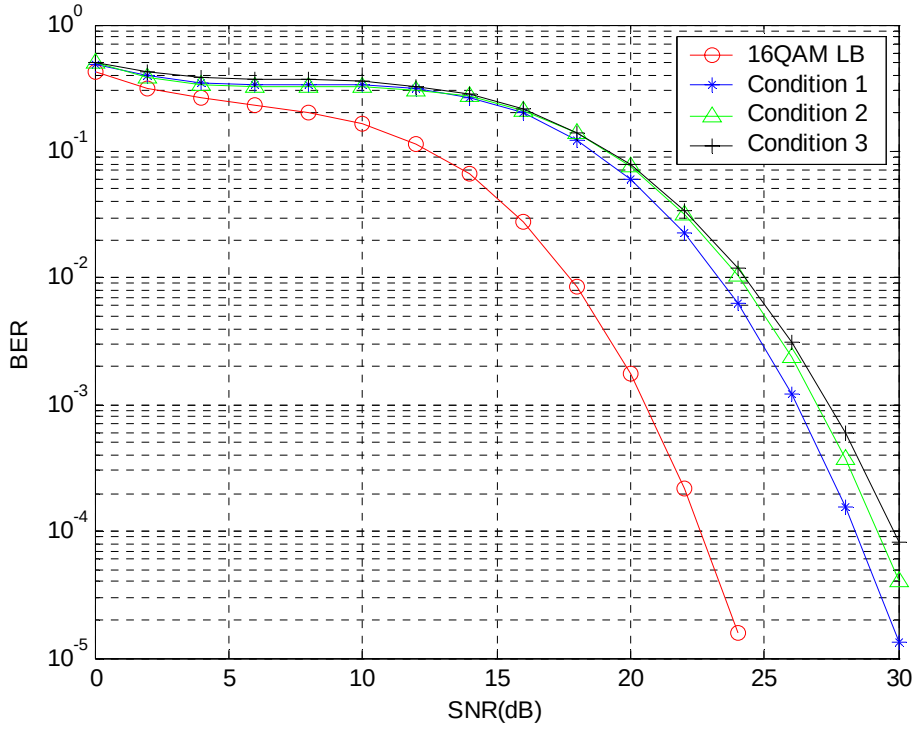

Fig. 5-11 Comprehensive BER performance of 16QAM.

5.9 Summary

In this chapter various simulation results are illustrated to verify the proposed algorithm. When the received signal to be processed is only corrupted by ISI, I/Q mismatch and AWGN, the I/Q mismatch canceller can remove the I/Q mismatch very well and improve the BER performance dramatically compared to no I/Q mismatch canceller, as shown in Fig. 5-1. When the received signal is only corrupted by varying DC offset $\tilde{\boldsymbol{d}}(n)$, constant DC offset $\bar{\boldsymbol{d}}(n)$ and AWGN, by employing the DC offsets canceller, these two kinds of DC offsets can be removed successfully, as shown in Fig. 5-2. When the received signal is corrupted by ISI, I/Q mismatch, varying and constant DC offsets and AWGN, the performance of the I/Q mismatch canceller and the DC offsets canceller still can work very well, as discussed in Section 5.5. The importance of the CDFE in the proposed algorithm is illustrated in Section 5.6. In addition, the efficiency of the internal iterative algorithm which is used to accelerate the convergence and to mitigate the interactions among the adaptations of $\{m_i\}$, $\bar{\boldsymbol{w}}$, $\{\hat{\boldsymbol{w}}_j\}$ and $\{\breve{\boldsymbol{w}}_k\}$ is illustrated in Section 5.7. It is seen that the internal iterative algorithm can accelerate the convergence dramatically, as shown in Fig. 5-8. Moreover, when the received signal is corrupted all the mentioned distortions, the comprehensive performance of the proposed algorithm is discussed in Section 5.8. These simulation results show that the proposed algorithm can mitigate all the distortions very well.

CHAPTER 6

CONCLUSIONS AND FUTURE WORK

6.1 Conclusions

In this thesis, an adaptive algorithm is proposed to remove I/Q mismatch, DC offsets, flicker noise and ISI simultaneously in a direct conversion receiver. I/Q mismatch is cancelled by a real valued adaptive mismatch canceller according to the model in Chapter 2. In addition, DC offsets are removed with one complex tap. The method has been verified by some papers and the simulations in Section 5.4 verify it too. Moreover, flicker noise is modeled as an AR random process, so the system to be identified transforms to an ARX model. After estimating the coefficients in the model during training period, the desired signal can be estimated by using decision feedback method. As illustrated in Chapter 5, the proposed algorithm is robust to I/Q mismatch, DC offsets and flicker noise.

Because of the interactions among the adaptations of $\{m_i\}$, $\bar{\boldsymbol{w}}$, $\{\hat{\boldsymbol{w}}_j\}$ and $\{\breve{\boldsymbol{w}}_k\}$, as shown in Section 3.4, an internal iterative algorithm is introduced to accelerate the convergence of the algorithm and to mitigate the interactions among the adaptations of the different groups of the taps in Section 3.5. As illustrated in Section 5.7, the learning curve of the MSE can converge much faster due to the proposed internal iterative algorithm.

In addition, the convergence of the mean of the taps is discussed in Chapter 4.

6.2 Future Work

In this thesis an integrated adaptive filter and equalizer is proposed to mitigate the distortions caused by I/Q mismatch, DC offsets, flicker noise and ISI. The proposed adaptive filter and equalizer is composed of a mismatch canceller, a DC offsets canceller, a CFFE and a CDFE in sequence. Due to the complicated structure of the filter, there are many mathematical analyses that are not covered by this thesis within the limited time.

Firstly, because the interactions among the adaptations of the different groups of the taps, the proposed algorithm is nonlinear, so the filter may result in biased optimum coefficients for I/Q mismatch canceller and CFFE. This biased estimation of the taps may degrade the performance of the algorithm. The analysis of the issue should be done to find the negative influence of the biased estimation on the performance of the algorithm.

Secondly, in the thesis an internal iterative algorithm is introduced to accelerate the convergence of the algorithm and to mitigate the interactions among the adaptations of the different groups of the taps. Simulation result shows that the internal iterative algorithm can accelerate the convergence of the algorithm dramatically. Mathematical analysis of the internal iterative algorithm to reduce the negative influence caused by the

interactions among the adaptations of the different groups of taps should be done in the future.

Thirdly, in this thesis, only the convergence of the mean of the taps is discussed. As we know, the independent assumption is based on the assumption that the step size is very small, thus the results obtained based on the independent assumption are also questionable. It is more meaningful to derive the convergence of the variances of the elements of the taps to some limited values.

Finally, the mathematical derivation of the minimum mean-square-error (MMSE) is needed in the future work. In addition, the expression of the misadjustment is also needed. According to the misadjustment, we can choose suitable step sizes to adjust the taps of the filter.

REFERENCES

[1] B. Razavi, "Design Considerations for Direct-Conversion Receivers," IEEE Trans. Circuits and Systems-II: Analog and Digital Signal Processing, Vol. 44, No.6, pp.428-435, 1997.

[2] W. Namgoong and T. H. Meng, "Direct-Conversion RF Receiver Design," IEEE Trans. Commun., Vol. 49, No.3, pp. 518-529, 2001.

[3] M. Faulkner, "DC offset and IM2 removal in direct conversion receivers," IEE Proc. Commun., Vol. 149, No.3, pp. 179-184, 2002.

[4] J. K. Cavers and M. W. Liao, "Adaptive Compensation for Imbalance and Offset Losses in Direct Conversion Transceivers," IEEE Trans. Vehicular Technology, Vol. 42, No. 4, pp. 581-588, 1993.

[5] B. Razavi, "RF IC design challenges," in Proc. Design Automation Conf., San Francisco, CA, pp. 408-413, 1998.

[6] A. A. Abidi, "Direct-conversion radio transceivers for digital communications," IEEE J. Solid-State Circuits, Vol. 30, pp.1399-1410, 1995.

[7] B. Lindoff, "Using a Direct Conversion Receiver in EDGE Terminals-a New DC Offset Compensation Algorithm" in Proc. The 11th IEEE International Symposium on Personal, Indoor and Mobile Radio Comm., Vol. 2, 2000, pp. 959-963.

[8] H. Yoshida, H. Tsurumi and Y. Suzuki, "DC Offset Canceller in a Direct Conversion Receiver for QPSK Signal Reception," in Proc. The Ninth IEEE International Symposium on Personal, Indoor and Mobile Radio Comm., Vol. 3, pp. 1314-1318, 1998.

[9] C. Mingzheng, Z. Yuanjin and H.K. Garg, "A Novel Adaptive Equalizer and Compensator for Direct Conversion Receivers," in Proc. The Ninth IEEE Singapore International Conference on Communications System, pp. 436-440, 2004.

[10] L. Ljung, System Identification: theory for the user, Second Edition, Prentice Hall PTR, 2002.

[11] B. Farhang-Boroujeny, Adaptive filters: theory and applications, John Wiley & Sons Ltd, 1998.

[12] C. Mingzheng, Z. Yuanjin and H.K. Garg, “A Novel Algorithm for DC Offsets and Flicker Noise Cancellation in Direct Conversion Receivers,” in Proc. The Ninth IEEE Singapore International Conference on Communications System, 6-8 September 2004, Singapore. pp. 441-445. Singapore: IEEE Singapore Section.

[13] John G. Proakis, Digital Communicationis, Fourth Edition, McGRAW-HILL INTERNATIONAL EDITION, 2001.

[14] S. Haykin, Adaptive Fitler Theory, Fourth Edition, Publishing House of Electronics Industry, 2002.

[15] S. Serbetli and A. Yener, “Transceiver Optimization for Multiuser MIMO Systems,” IEEE Trans. Signal Processing, Vol. 52, No.1, pp. 214-226, 2004.

LIST OF PUBLICATIONS

[1] Yuanjin Zheng, Mingzheng Cao and H.K.Garg. A Novel Adaptive Equalization and Cancellation Algorithm for Direct Conversion Receivers. in Proc. The Fourth International Conference on Information, Communication & Signal Processing/Fourth IEEE Pacific-Rim Conference on Multimedia, 15-18 December 2003, Singapore. pp. 1-5. Singapore: IEEE Singapore Section.

[2] Mingzheng Cao, Yuanjin Zheng and H.K.Garg. A Novel Adaptive Equalizer and Compensator for Direct Conversion Receivers. in Proc. The Ninth IEEE Singapore International Conference on Communications System, 6-8 September 2004, Singapore. pp. 436-440. Singapore: IEEE Singapore Section.

[3] Mingzheng Cao, Yuanjin Zheng and H.K.Garg. A Novel Algorithm for DC Offsets and Flicker Noise Cancellation in Direct Conversion Receivers. in Proc. The Ninth IEEE Singapore International Conference on Communications System, 6-8 September 2004, Singapore. pp. 441-445. Singapore: IEEE Singapore Section.